Title: Temporal profiling of *Salmonella* transcriptional dynamics during macrophage infection using a comprehensive reporter library

Authors:

Taylor H. Nguyen[1,*], Oscar R. Diaz[2,*], Manohary Rajendram[1], Daniel S.C. Butler[2], Benjamin X. Wang[2], Jay C. D. Hinton[3], Denise Monack[2,†], Kerwyn Casey Huang[1,2,4,†]

Affiliations:

[1]Department of Bioengineering, Stanford University, Stanford, CA 94305

[2]Department of Microbiology and Immunology, Stanford University School of Medicine, Stanford, CA 94305

[3]Institute of Infection, Veterinary & Ecological Sciences, University of Liverpool, Crown Street, Liverpool, L69 7ZB, United Kingdom

[4]Chan Zuckerberg Biohub, San Francisco, CA 94158

[*]: co-first authors

[†]: correspondence to kchuang@stanford.edu (K.C.H.) and dmonack@stanford.edu (D.M.)

Keywords: *transcriptional reporter fusions; transcriptomics;* in vitro *screening; systems biology; macrophage; SPI2; Entner-Doudoroff pathway; population-level heterogeneity; manganese; metal homeostasis*

Abstract

The transcriptome of *Salmonella enterica* serovar Typhimurium (*S*. Tm) dynamically responds to the rapid environmental shifts intrinsic to *S.* Tm lifestyle, exemplified by entry into the *Salmonella*-containing vacuole (SCV) within macrophages. Intracellular *S*. Tm must respond to the acidity of the SCV, accumulation of reactive oxygen/nitrogen species, and fluctuations in nutrient availability. Despite thorough RNA-seq-based investigations, the precise transcriptional timing of the expression of many secretion systems, metabolic pathways, and virulence effectors involved in infection has yet to be elucidated. Here, we construct a comprehensive library of GFP-reporter strains representing ~3,000 computationally identified *S.* Tm promoter regions to study the dynamics of transcriptional regulation. We quantified promoter activity during *in vitro* growth in defined and complex media and throughout the timeline of intracellular infection of RAW 246.7 macrophages. Using bulk measurements and single-cell imaging, we uncovered condition-specific transcriptional regulation and population-level heterogeneity in the activity of virulence-related promoters, including SPI2 genes such as *ssaR* and *ssaG*. We discovered previously unidentified transcriptional activity from 234 genes, including ones with novel activity during infection that are associated with pathogenecity islands and are involved in metabolism and metal homeostasis. Our library and data sets should provide powerful resources for systems-level interrogation of *Salmonella* transcriptional dynamics.

Introduction

Salmonella serovars are responsible for human diseases ranging from gastroenteritis to systemic infections. *Salmonella enterica* serovar Typhi only infects humans and is responsible for typhoid fever, while *Salmonella enterica* serovar Typhimurium (*S*. Tm) has a broad host range and can survive in the wider environment. *S*. Tm infections usually result in self-limiting gastroenteritis in humans and systemic typhoid-like disease in mice[1]. *Salmonella* infections, which account for ~50% of foodborne illnesses worldwide[2], typically result from exposure to contaminated food or water. The emergence of multidrug-resistant *Salmonella* strains is now posing a major global health risk[3–6]. During systemic *Salmonella* infections, the pathogen penetrates the gut epithelial barrier and preferentially infects phagocytes within the lamina propria[7]. The ability of *Salmonella* to proliferate within macrophages in the *Salmonella*-containing vacuole (SCV) is a hallmark of systemic disease[8].

S. Tm can invade macrophages via upregulation of *Salmonella* pathogenicity island 1 (SPI1), which encodes the type 3 secretion system 1 (T3SS-1), associated virulence effectors, and regulators[9]. Following entry into macrophages, *S*. Tm cells respond to the nutrient-restricted and acidified environment of the SCV through transcriptional upregulation of *Salmonella* pathogenicity island 2 (SPI2) and expression of the type 3 secretion system 2 (T3SS-2), which leads to injection of *S*. Tm-derived virulence factors[10]. These virulence factors contribute to a variety of outcomes including skewing of macrophage polarization state, formation of *Salmonella*-induced filaments (elongated tubes that protrude from the SCV to enhance nutrient acquisition), modification of the SCV environment to minimize bacterial clearance, and inhibition of antibacterial pathways within the host cell[10].

Quantification of the *S*. Tm transcriptome using RNA-seq revealed patterns of gene regulation under a variety of *in vitro* conditions and during macrophage infection[11–13]. Previous studies

suggested that *S.* Tm responds to the macrophage intracellular environment by shifting from initial expression of genes within SPI1 to subsequent expression of SPI2 genes in the first 8 h of infection, coinciding with a transcriptional shift of the infected host macrophage[14]. An outstanding challenge is to understand the physiological adaptations and transcriptional dynamics that occur in *S.* Tm throughout intracellular replication, especially during host metabolic reprogramming and nutrient sequestration[15].

Through an intricate regulatory network, *Salmonella* can adapt its transcriptional program within 4 min upon encountering a new environment[16]. Given the short half-life of mRNA transcripts[17], capturing response dynamics with a high temporal resolution is vital. Furthermore, the identification of additional virulence-related genes and determination of their expression dynamics during infection remain important challenges, and a deeper understanding of the transcriptional response of *Salmonella* to various environmental perturbations should empower development of antimicrobial treatments to *Salmonella* infection. Technical limitations and the expense of RNA-seq are obstacles to measurement of the genome-wide transcriptional profile with high temporal resolution. An alternative transcriptional profiling approach involves engineering strains in which a promoter is fused to a reporter, such as a fluorescent protein, to enable measurement of promoter activity over time. This approach has been facilitated by the development of highly stable, fast-folding GFP variants that avoid delays in activity read-out[18]. A comprehensive library of such promoter reporters was constructed and used to quantify the dynamics of the *Escherichia coli* transcriptome, enabling the discovery of transcriptional regulatory regions[19,20]. Previous studies using *S.* Tm promoter reporters were targeted to specific pathways of interest such as the response of biofilm-associated promoters to biofilm inhibitors, of metabolic genes upon entry into the SCV, and stress responses during intracellular infection[21–23]; a comprehensive characterization of the dynamics of the *S.* Tm transcriptome has not been conducted.

Here, we report the construction of a comprehensive reporter library containing ~3,000 promoter regions identified from the *S.* Tm genome fused to GFP and its application to measuring the dynamics of *S.* Tm transcriptional regulation. We profiled changes in *S*. Tm promoter activity across defined and complex media conditions, capturing condition-specific regulation of promoters and the global response to *in vitro* conditions that mimic aspects of the intra-macrophage environment. Using fluorescence microscopy, we demonstrate that our library can be used to quantify heterogeneity in promoter activity across a population of single bacterial cells. To determine the transcriptional response of *S*. Tm to the intracellular macrophage environment, we used time-lapse fluorescence microscopy of RAW 264.7 macrophage-like cells infected with each reporter strain in the library individually. Our experimental screens provided the first evidence of activity for 234 promoters. We found that the *mntS* promoter region is dependent on environmental manganese concentrations and is active during macrophage infection, highlighting the importance of metal homeostasis during pathogenesis. By capturing transcriptional dynamics, we identified a metabolic shift in *S.* Tm to the Entner-Doudoroff (ED) pathway during the later stages of intracellular infection. In total, our library and analyses uncovered temporal patterns of transcriptional regulation involving *S*. Tm genes related to metabolism, metal acquisition, and pathogenicity.

Results

Construction of a comprehensive library of Salmonella *Typhimurium transcriptional reporters*

Our goal was to construct a comprehensive arrayed library of GFP reporter fusions to every lead-operon (primary) promoter in *S.* Tm. To this end, we identified 2,901 promoters using an unbiased computational approach. First, we extracted the intergenic distances between NCBI-annotated coding sequences (CDS) across the *S.* Tm strain SL1344 genome. Genes with intergenic distances <40 bp were considered to be transcribed as part of an operon and were excluded from further analysis. For the remaining 2,901 CDS, we defined the promoter region as the 350 bp upstream of and including the translational start site (TSS, start codon). Of these primary promoters, the transcriptional start sites of 1,850 were experimentally validated in previous studies that enriched for *S.* Typhimurium 4/74 primary transcripts via differential RNA-seq (dRNA-seq)[13]. The remaining 1,051 were considered putative. We did not consider potential promoters within genes or regulation that occurs from sequences after the start codon. We did not include regions downstream of the TSS because we reasoned that including the N-terminal signal sequence that translocates proteins to the periplasmic space and the inner/outer membrane would interfere with the folding and stability of our GFP fusion, a hypothesis that was borne out for a small set of randomly selected membrane proteins (**Fig. S1**). The final reporter constructs in our library, which contain the promoter regions followed by the *mGFPmut2* sequence[18], were cloned into a common plasmid backbone that includes the pSC101 origin of replication, the *mob* mobilization region to enable conjugative transfer between strains, and a chloramphenicol-resistance (Cm^R) cassette (**Fig. 1A**).

Plasmids were assembled, sequence verified, and arrayed into 96-well plates. Using a high-throughput cloning strategy in 96-well plates (**Methods**), the arrayed plasmid library was

transformed into chemically competent *E. coli* NT11164 (**Table S1**), a strain that requires diaminopimelic acid for growth and contains an integrated high-frequency recombination plasmid for conjugation into *S.* Tm[24] (**Fig. 1B**, **Methods**). The plasmids were then conjugated into a *S.* Tm SL1344 strain containing the *dTomato* gene (which encodes the fluorescent protein dTomato) at the *phoN* locus, an established reporter that is up-regulated by >50-fold during intracellular macrophage infection[13,25]. This *S.* Tm SL1344::*phoN-dTomato* strain retains comparable infectious capacity to wild-type *S.* Tm *in vivo*[26,27]. Library construction resulted in successful cloning of 99.1% (2,874 of 2,901) of the reporter plasmids into *S*. Tm. We sequence verified the promoter region of a randomly selected subset of ~150 strains including ones that were the focus of follow-up experiments (**Table S2**); the expected identify was confirmed in almost all cases, and mismatches attributed to human error during colony picking were not used for downstream analyses. Our *E. coli* collection of *S.* Tm reporter plasmids is stored in 96-well format to simplify future conjugation into other strains of interest, and the final arrayed library of GFP reporter fusions in *S.* Tm SL1344::*phoN-dTomato* enables the interrogation of *S.* Tm transcriptional dynamics and regulation using high-throughput screens in a fluorescence plate reader or via microscopy, as we demonstrate below.

Profiling* S. *Tm transcriptional dynamics across* in vitro *conditions

To profile infection-relevant transcriptional programming, we characterized our library during *in vitro* growth in media that represent the key physiochemical aspects of the intracellular macrophage environment. Previous work probing the *Salmonella* transcriptional response used a defined minimal medium to replicate the low pH, low phosphate (P_i), low magnesium (Mg^{2+}), and low nutrient features of the SCV, an intracellular environment within macrophages that induces expression of SPI2[12,28]. Hence, we screened the library in the following defined media: NonSPI2 (pH 7.4, 25 mM P_i, 1 mM MgSO4), InSPI2 (pH 5.8, 0.4 mM P_i, 1 mM MgSO4), and InSPI2 low Mg (pH 5.8, 0.4 mM P_i, 10 μM $MgSO_4$). We also screened the library in 10% Brain

Heart Infusion (BHI) to probe transcription in a gut-relevant setting[29], hypothesizing that this rich (undefined) medium would reveal distinct transcriptional programming. Measurements of reporter activity were carried out in a fluorescence plate reader in 384-well black-walled plates by measuring OD_{600} and GFP every ~10 min over 24 h to generate an *in vitro* data set containing >3.3 million data points.

Virtually all strains in the promoter library exhibited growth kinetics similar to wild-type *S.* Tm (**Fig. 1C**), indicating that the presence of the reporter plasmid does not affect fitness. We quantified the activity of each promoter (hereafter referred to for a given gene as P*gene*) based on the background-subtracted GFP signal (difference between the fluorescence of the strain of interest and the autofluorescence of the parent strain without a plasmid), normalized by background-subtracted OD_{600} to account for changes in cell density. A promoter was defined as "ON" based on comparison to a dynamic estimate of background noise (**Fig. S2**, **Methods**).

The time at which promoter activity was first considered ON (t_{ON}) was broadly distributed across library strains and conditions (**Fig. 1D**), suggesting that the library can probe transcriptional dynamics in all phases of growth from lag to stationary. In NonSPI2, t_{ON} exhibited a bimodal distribution, with the second peak consisting of reporters for genes related to stationary phase such as *dps* (t_{ON}=8.8 h) and *cstAa* (t_{ON}=11.9 h), which encode proteins responsible for DNA protection in stationary phase[30] and escape from carbon starvation[31], respectively. 64.4% (1,850 of 2,874) of the strains in our library were ON in at least one *in vitro* condition. 50.1% (1,440) of the strains turned ON in NonSPI2, 41% (1,177) in InSPI2, 37.9% (1,089) in InSPI2 low Mg, and 50.6% (1,454) in 10% BHI. Based on the maximum activity across all time points in each of the four conditions, promoters clustered into condition-specific profiles (**Fig. 1E**).

To evaluate the efficacy of our library, we compiled a list of genes related to SP1, T3SS-1, SPI2, and T3SS-2 (**Table S3**) and quantified their activity in the four *in vitro* conditions. Promoters from the SPI2 pathogenicity island (e.g., *orf7*, *orf319*, *ssaG*, *ssaR*, *ssrA*) (**Fig. 1F**), regulators (e.g., *phoP*, *hilA*, *ompR*, *sirC*), structural proteins (e.g., *ompC*, *ompF*, *sicA*), effectors (e.g., *cigR*, *gtgE*, *pipB*, *pipB2*, *sifB*, *sopD2*, *sopE*, *sseJ*, *sseK3*, *sspH2*, *steA*), and other miscellaneous proteins (e.g., *phoN*, *pagC*, *pagO*, *pagD*, *pagK*) that are canonically up-regulated during infection showed high activity (**Fig. S3**), particularly in the InSPI2 conditions (high or low Mg)[12,28,32]. However, contrary to expectations from RNA-seq measurements[12], some reporters (*ssaB*, *ssaM*, *sscB*) did not exhibit activity in InSPI2 media, indicating that these individual constructs may be missing key regulatory sites. Thus, for downstream analyses, we focused on the reporters with positive signal rather than potential false negatives.

In addition to promoter activity dynamics, the strains in our library enable quantification of population-level heterogeneity in gene expression (e.g., via flow cytometry or single-cell imaging). Previous work showed that some *Salmonella* virulence factors are expressed heterogeneously across single cells, and this phenotypic variation can play an integral role in *Salmonella* virulence[33]. For example, upon SCV invasion, a subpopulation of *Salmonella* cells transition into a non-replicating persister state that can better withstand long-term host-induced damage and antibiotic treatment[34]. Hence, we sought to quantify population-level heterogeneity for five SPI2-operon promoters that turned ON in InSPI2 conditions. We collected fluorescence images of >1,000 cells for each strain after 8 h of growth (approximately when these promoters reached maximum activity in InSPI2) in NonSPI2, InSPI2, and InSPI2 low Mg and quantified the distribution of GFP fluorescence intensity across the population (**Fig. 1G**). These strains displayed a wide range of population-level behaviors. P*orf7* cells exhibited a relatively narrow distribution of GFP fluorescence intensities, whereas P*ssaR* cells exhibited a wide range of intensities that spanned more than two orders of magnitude (**Fig. 1H**). These data also confirmed that the P*orf7*

212 reporter, whose bulk signal was only slightly above our background noise threshold, indeed turned
213 ON at the single cell level, providing confidence for the positive hits from our bulk screen that
214 were near the background threshold. These results demonstrate that our library and experimental
215 setup produces the expected induction of several genes in the tightly regulated SPI2 pathogenicity
216 island, and that the reporters enable quantification of *in vitro* transcriptional dynamics through
217 bulk and single-cell measurements.
218
219 ***Distinct* Salmonella *promoter activity dynamics in infection-relevant media***
220 In the four growth conditions, the reporter strain library exhibited a wide range of maximum
221 promoter activities and of times to reach maximum activity (t_{max}) (**Fig. 2A**). Maximum activity was
222 not correlated with t_{max}, emphasizing the importance of quantifying the full range of dynamic
223 behaviors to comprehensively profile *S.* Tm transcriptional activity. We focused on the 895
224 promoters that turned on in all three SPI2 conditions (NonSPI2, InSPI2, InSPI2 low Mg) (**Fig. 2B**)
225 and compared activity normalized to its maximum across reporters. Clustering of normalized
226 promoter activity in NonSPI2 revealed sets of promoters with qualitatively distinct patterns (e.g.,
227 constitutive, late, pulsatile) (**Fig. 2C**). Ordering the strains by t_{max} revealed that promoters
228 collectively reached maximum activity across the entire 24 h in NonSPI2 (**Fig. 2D, left**). To
229 compare dynamic behaviors across conditions, the same analyses were performed for promoter
230 activity in InSPI2 and InSPI2 low Mg (**Fig. 2D**). In contrast to NonSPI2, t_{max} values in InSPI2 and
231 InSPI2 low Mg were much more narrowly distributed. In these two conditions, reporter responses
232 resembled a pulse in which activity decreased dramatically after reaching a maximum at ~10 h
233 (**Fig. 2D, middle and right**), with t_{max} for many promoters shifted to an earlier stage of growth
234 compared with NonSPI2. Thus, *S.* Tm displays distinct transcriptional dynamics in SPI2-inducing
235 versus non-inducing conditions.
236

We sought to elucidate the basis of the pulse. Pulsatile behavior still occurred when an antibiotic was added to maintain plasmid selection and in 96-well (rather than 384-well) plate formats (data not shown), suggesting that the decrease in GFP at later times was not due to plasmid loss or poor oxygenation, respectively. We noted that maximum promoter activity in InSPI2 and InSPI2 low Mg occurred approximately coincident with cells entering stationary phase, and we hypothesized that cells underwent a physiological shift during this transition. Single-cell imaging after 24 h of growth in InSPI2 or InSPI2 low Mg revealed cells with disrupted morphologies, whereas cell morphology was normal after 24 h of growth in NonSPI2 (**Fig. S4A**). In InSPI2, after 24 h cells contained regions that were less phase dark, which were likely regions where the outer membrane was separated from the cell wall[35] (**Fig. S4A**). During growth in InSPI2 low Mg in 12-well plates, cell cultures exhibited lysis after 24 h of growth (**Fig. S4B**), likely due to the role of Mg^{2+} in outer membrane stabilization[36]. Although buffered, pH decreased in all three SPI2 media after 24 h of growth (**Fig. S4C**), which could compound stationary-phase stress. These results reveal that *S.* Tm physiology is strongly impacted by growth in InSPI2, particularly during the transition to stationary phase, and these factors should be considered when evaluating any phenotypes in these media.

This global shift in promoter activity profiles in SPI2-inducing conditions led us to hypothesize that in addition to the known up-regulation of SPI2-related gene activity, there is also time-dependent regulation in response to environmental stimuli, especially prior to cells entering stationary phase. Indeed, for the vast majority of reporters for SPI2-related genes that were active in all 3 SPI2 media, including *ssrA*, *ompC*, *ompF*, *ssaG*, *ssaR*, *sseJ*, *pipB*, *sopD2*, *pipB2*, and *sspH2*, t_{ON} was earlier in InSPI2 and InSPI2 low Mg compared with NonSPI2 (**Fig. 2E,F**). Transcription of *phoP*-activated genes is known to be regulated by magnesium levels[3997], and indeed t_{ON} for the *phoP*, *phoN*, *pagC*, and *pagD* reporters was shifted earlier in InSPI2 low Mg compared to InSPI2 (**Fig. 2E,F**). Some other SPI2-related reporters, such as *sifB*, were induced in SPI2-inducing media but

not in NonSPI2 (**Fig. 2F**). Taken together, these *in vitro* data demonstrate that our reporter library can capture systems-level changes in activity and dynamic regulation in conditions designed to mimic aspects of the intra-macrophage environment.

Salmonella ***promoters turn on in multiple stages during macrophage infection***

Our *in vitro* data demonstrate that we can capture time-dependent transcriptional regulation, and we next sought to profile such regulation in *S.* Tm within macrophages. To achieve this goal, we infected a macrophage-like cell line with each strain in our library individually and measured intracellular fluorescence via time-lapse fluorescence microscopy coupled to automated cell segmentation. The parent strain (SL1344::*phoN-dTomato*) expresses dTomato within a macrophage, enabling normalization of the GFP signal to bacterial cell density during infection (**Methods**)**.** Intracellular reporter activity was measured using a high-throughput fluorescence microscope (**Methods**). Images were collected from each well in a 96-well black-walled plate in phase and two fluorescence channels (GFP and dTomato) every ~1 h over 24 hours post infection (h.p.i.). Following automated macrophage segmentation, intracellular reporter activity was quantified for *S*. Tm-positive macrophages, which generated an infection dataset containing >730,000 data points. To classify strains based on phases of the host-pathogen response, we binned infection into four stages: early (0–4 h.p.i.), middle (5–9 h.p.i.), late (10–12 h.p.i.), and escape (13–15 h.p.i.) (**Fig. 3A**).

During infection, a promoter was defined as “ON” based on comparison to a dynamic estimate of background noise over the 1–15 h.p.i. interval (**Fig. S5**). Normalization by the fluorescence signal from the dTomato transcriptional reporter was not performed until 4 h.p.i. since SCV maturation is needed to induce *phoN* expression. Hence, during the early stage of infection (1–4 h.p.i.), we quantified activity of each promoter as the background-subtracted GFP signal (difference between the mean GFP fluorescence for GFP-positive macrophages infected by the strain of interest and

the mean GFP fluorescence for all macrophages of the parent strain without a plasmid). Promoter activity during the middle, late, and escape stages (5–15 h.p.i.) was quantified as the background-subtracted GFP signal (difference between the mean GFP fluorescence for dTomato-positive macrophages infected by the strain of interest and the mean GFP fluorescence for all macrophages of the parent strain without a plasmid), normalized by background-subtracted dTomato fluorescence from dTomato-positive macrophages to account for intracellular bacterial replication (**Methods**).

In total, 1,007 promoters were detected as ON during the first 15 h of macrophage infection. There was a wide range of dTomato-normalized GFP signal, and 41% of promoters turned ON prior to 5 h.p.i (**Fig. 3B**). The distribution of time to reach maximum activity (t_{max}) was multimodal, spanned the 15 h of intracellular infection, and was not correlated with maximum promoter activity (**Fig. S6A**). The distribution of maximum promoter activity was log normal, indicating that most promoters exhibited relatively low activity while a few displayed very high activity (**Fig. S6B**). As expected, the promoter regulating *phoE* (SL1344_0316/SL1344_RS01640), which encodes a phosphate-limitation-inducible outer membrane porin, exhibited the highest activity upon invasion, reflecting the essentiality of the *S.* Tm response to the phosphate-limited intracellular environment[38] (**Fig. S6C**). We observed promoters turn ON at every hour of infection, reflecting the dynamic programming of *S.* Tm's response throughout intracellular infection (**Fig. 3C**). The first peak in t_{ON} reflects the expected large pulse in promoter activity by invading *S.* Tm to the intracellular environment during the early stage of infection (1–4 h.p.i.)[11]. The distribution of t_{ON} values exhibited a second peak at 5 h.p.i. following maturation of the SCV and accumulation of host derived reactive oxygen species (ROS)[8,39,40] (**Fig. 3C**).

Previous studies documented a precise transcriptional timing pattern for the genes contained within SPIs during macrophage infection[11,13,41]. Specifically, *S.* Tm invasion of macrophages

initiates through the upregulation of SPI1 genes that encode the T3SS-1, associated virulence effectors, and regulators[42]. This early stage of infection captures initial *S*. Tm invasion and formation of the SCV[8,43]. Interestingly, prior to invasion several promoters of genes within the SPI1 locus (e.g., *sirC*, *SL1344_2880/SL1344_RS15015*) exhibited high activity when localized near macrophages during the early stage of infection[44,45] (**Fig. 3D**). We observed that SPI1 promoters exhibited heterogeneity in GFP signal in extracellular *S*. Tm cells (**Fig. 3D**), consistent with previous findings[46,47]. These results show that our library can expand our understanding of heterogeneity across virulence-related promoters.

Following entry of *S*. Tm into macrophages, previous studies showed that acidification of the SCV results in SPI2 upregulation and production of the T3SS-2, which leads to injection of additional effector proteins[48,49]. This middle stage (5–9 h.p.i.) captures the *S*. Tm response to host cell oxidative and nitrosative bursts, maturation of the SCV, and expression of the pathogenicity islands relevant to intracellular replication[39,40]. As expected, the promoters of genes associated with the SPI2 T3SS-2 (e.g., *ssaG*, *ssaR*, *sifB*, *pipB*, *pipB2*) and other virulence-related genes (e.g., *phoP*, *ompC*, *ompF*, *sopD2*, *sseJ*, *sspH2*, *steA*) exhibited high activity during intracellular macrophage infection (**Fig. 3E, S7**). Thus, SPI1 and SPI2 are largely activated sequentially during macrophage infection.

Another common strategy for the genetic acquisition of virulence effectors in *S*. Tm involves phage-mediated integration into the core genome using the content of prophage islands to express effectors required for intracellular replication or survival[50]. However, the precise timing of the transcriptional activation of these loci remains unclear. We observed that the promoters for virulence effectors GtgE (encoded on the Gifsy-2 prophage) and SseK3 (encoded on the ST64B prophage) were active during the middle stage of infection (t_{ON}=6 h for both)[50,51] (**Fig. 3F**). Furthermore, the expected timing of ROS accumulation in infected macrophages 5–7 h.p.i.[40] was

followed by increased activity of promoters regulating expression of the SOS response: regulator *recA* (t_{ON}=8 h), several superoxide dismutases that are important antioxidants for minimizing ROS-mediated damage (e.g., *sodA,* t_{ON}= 6 h; *sodB*, t_{ON}=7 h; *sodCa*, t_{ON}=5 h; *sodCb*, t_{ON}=7 h), and other genes related to resistance to oxidative damage (e.g., *ahpF*, t_{ON}=5 h)[52] (**Fig. 3G, S8A**).

During the late stage of infection (10–12 h.p.i.), we expected activity from promoters of genes in response to the continued accumulation of ROS in macrophages and ones needed to prime *S*. Tm for the upcoming host lysis and escape[53]. Indeed, we observed genes related to oxidative damage turn ON in the late stage, such as alkyl hydroperoxide reductase[52] (*ahpC*, t_{ON}=11 h) (**Fig. 3H**). We also observed activity onset for sigma factor *rpoE* (t_{ON}=10 h) whose deletion has been found to sensitize *S*. Tm to killing by antimicrobial peptides and ROS[54] (**Fig. S8A**). The promoter of *pgtE*, which encodes an outer membrane protease responsible for complement cleavage[55], turned ON at 12 h, likely to prime *S*. Tm for the extracellular environment, (**Fig. 3H**). Additionally, several prophage gene promoters (e.g., *gpE*, *gpO*, *pspA*, and *pspB*) exhibited high activity during the later stages of macrophage infection (**Fig. S8B**).

Lastly, we examined *S.* Tm promoter activity during the escape stage of macrophage infection between 13–15 h.p.i., an interval during which macrophages undergo inflammasome-mediated pyroptosis[56]. The promoter for *yihO*, which encodes a membrane transport protein important for capsule assembly and environmental persistence[57], turned ON during the later stages of infection (t_{ON}=13 h), as did *araC,* part of the L-arabinose utilization operon that is important for the carbohydrate metabolism in the gut environment[58]. In summary, mapping the dynamics of transcriptional regulation during macrophage infection corroborated previous findings regarding the early response of *S*. Tm to the intracellular environment[11,59,60], and provided the precise timing of activation for promoters regulating the expression of virulence-related genes over each stage of infection.

367

368 ***Comparative analysis between* in vitro *growth and intracellular infection identifies novel***
369 ***infection-relevant promoters***

370 In total, 70.1% (2,016 of 2,874) of the reporter strains were defined as ON in at least one *in vitro*
371 condition and/or during intracellular macrophage infection. By constructing strains for all
372 computationally predicted promoters, our reporter library was able to provide the first experimental
373 validation of some promoters. To generate this list, we first compared to previous RNA-seq results
374 representing a compendium of conditions for potential gene activation, and we manually removed
375 promoters from this list that our literature search identified as confirmed by other methods such
376 as 5´RACE (**Table S4**). Our screens report novel activity for 234 promoters that can be divided
377 into two groups (**Fig. 4A)**. In the first group, 112 (out of 283 putative promoters) are considered
378 "newly identified promoters" because they were not included in previous RNA-seq analyses and
379 thus do not have currently available transcriptomics information due to the use of an older (less
380 well annotated) reference genome[12,13]. In the second group, 122 (out of 249) are considered
381 promoters of "newly identified activity" since these regions did not exhibit activity across 22 *in vitro*
382 conditions or during intracellular macrophage infection in previous RNA-seq studies[12,13]. The 234
383 promoters with novel activity that emerged from our screen encompass a wide range of condition-
384 specific activity across the four *in vitro* media and intracellular infection conditions (**Fig. 4B**) and
385 represent diverse biological processes (**Fig. 4C, Methods**).

386

387 Among the "newly identified promoters," the reporter for *mntS* (SL1344_RS25090) exhibited high
388 activity in InSPI2 media (high and low Mg) and during intracellular macrophage infection. The
389 promoter region for *mntS* encodes a small (42 aa)[61] manganese (Mn^{2+}) response protein that is
390 predicted to be involved in metal homeostasis, but has not been studied previously in *S*. Tm. In
391 *E. coli*, MntS is important for maintaining Mn^{2+} levels in Mn^{2+}-limited environments[62] by inhibiting
392 the Mn^{2+}-exporter MntP[62]. Consistent with previous RNA-seq data[13], reporters for the Mn^{2+}

393 importer (P*mntH*), Mn^{2+}/iron importer (P*sitABCD*), and Mn^{2+} regulator (P*mntR*) exhibited activity
394 during intracellular macrophage infection (**Fig. 4D**). Our findings are consistent with adaptive
395 regulation of manganese levels by *S.* Tm in response to host Mn^{2+} sequestration in the SCV[63].
396
397 Given the *in vitro* and intra-macrophage activity of P*mntS* and other promoters related to Mn^{2+}
398 homeostasis, we hypothesized that P*mntS* would be sensitive to environmental Mn^{2+} levels.
399 Indeed, we found that P*mntS* exhibited a dose-dependent, anti-correlated response to
400 supplemented $MnCl_2$ concentration in InSPI2 in a range from 0–500 μM $MnCl_2$ (which includes
401 toxic concentrations that are known to activate export of Mn^{2+} through MntP and YiiP[64]) (**Fig. 4E**).
402 These findings are consistent with a previous study showing that MntS protein levels and
403 promoter expression levels are anti-correlated with environmental Mn^{2+} concentrations in *E.*
404 *coli*[61,65]. Our *mntP* and *yiiP* reporters did not show signal in any experiment (data not shown),
405 likely because these reporters are non-functional. Nonetheless, because P*mntS* activity was more
406 sensitive to Mn^{2+} levels than the regulator P*mntR* or importers P*mntH* and P*sitA*, we speculate
407 that MntS plays an important role in sensing and regulating intracellular Mn^{2+} levels in *S*. Tm.
408
409 Furthermore, our data set provided the first reported activity of many other promoters, 96 of which
410 are annotated with hypothetical functions (**Fig. 4C**, **Table S4**). Among these promoters with
411 "newly identified activity," we observed relatively high activity of the SopE-Phi prophage-
412 associated *P*SL1344_2718 during intracellular infection (**Fig. 4F**). Phyre2[66] predicted the structure
413 of SL1344_2718 to be a phage capsid protein with 100% confidence and 96% coverage.
414 Interestingly, this promoter did not turn ON in any of the *in vitro* conditions, illustrating a case of
415 macrophage-specific induction (**Fig. 4F**). These findings establish that our library is a powerful
416 tool for identifying promoters with previously unrecognized infection relevance, adding to the
417 repertoire of genes necessary for *Salmonella* to survive and replicate in the SCV environment.
418

Systems-level functional analysis reveals a metabolic pathway important for intracellular macrophage infection

Our identification of new promoter activity during infection, coupled with time-dependent intra-macrophage transcriptional regulation, suggested the potential to discover novel regulatory patterns crucial for intracellular survival. To determine links between promoter activity dynamics and *S*. Tm pathogenesis, we conducted a functional characterization of the 1,007 promoters induced during macrophage infection. The two largest groups involved promoters that regulate the expression of hypothetical and metabolism-related genes (**Fig. S9)**. Other pathways enriched during macrophage infection include transport, virulence, and the redox response, consistent with previous findings[13,41,60]. This analysis also highlighted the carbohydrate metabolism functional group, which includes promoters of genes in the Entner-Doudoroff (ED) metabolic pathway including *kdgK*, *kdgT*, *edd*, *eda*, *idnK*, *uxuA*, and *gnd*. The normalized fluorescence signal of several of these promoters first displayed activity between 8–15 h.p.i. (**Fig. 5A**). Since it is known that the ED pathway is upregulated during macrophage infection[11,21] and utilized to increase metabolic flux[67], we investigated the time-dependent regulation of this pathway. GFP fluorescence from the P*kdgK* reporter strain during macrophage infection increased after the increase in P*phoN*-regulated dTomato expression that reflected SCV maturation[8] (**Fig. 5B**).

Since the ED gene promoters exhibited increased activity in the middle, late, and escape stages of infection, we hypothesized that the ED pathway is important for intracellular *S*. Tm survival. The ED pathway is comprised of the enzymes 6-phosphogluconate dehydratase (encoded by *edd*) and KDGP aldolase (encoded by *eda*). The pathway culminates in aldol cleavage of 2-keto-3-deoxy-6-phosphogluconate (KDPG) into pyruvate to funnel into the tricarboxylic acid (TCA) cycle, ultimately contributing to energy production[68] (**Fig. 5C**). Consistent with our findings, a previous study using a *S.* Tm GFP reporter observed increased expression from the *edd* promoter within RAW macrophages[21]. Furthermore, isotope tracing of *S*. Tm metabolism during

445 macrophage infection revealed high metabolic flux through the ED pathway, which converts 6-
446 carbon sugars (e.g., hexuronates, gluconate, glucuronate, and galacturonate) into KDPG[67].
447
448 To validate the importance of the ED pathway during intracellular *S*. Tm replication, we individually
449 deleted the *kdgK*, *idnK*, and *uxuA* genes, which encode enzymes that feed metabolites into the
450 ED pathway. We measured bacterial replication rate using a previously developed dual-reporter
451 plasmid (pFCcGi)[69]. *S*. Tm Δ*kdgK*, Δ*idnK*, and Δ*uxuA* strains exhibited replication and growth
452 rates comparable to wild type across *in vitro* conditions, as did a Δ*kdgK* complementation strain.
453 The replication rate in macrophages was measured at 2, 6, and 10 h.p.i. using flow cytometry.
454 The mean fold-change in replication rate at 6 h.p.i. relative to 2 h.p.i. was similar (~1.6–1.8x
455 increase) across all strains (**Fig. 5D**), while a Δ*ssaV* strain deficient in SPI2 T3SS replicated
456 significantly less than wild type in macrophages, as previously reported[70]. The Δ*idnK* and Δ*uxuA*
457 strains, which lack genes encoding a D-gluconate kinase and mannonate dehydratase,
458 respectively, exhibited high variance in intracellular replication but were not significantly different
459 from wild type. Importantly, deletion of *kdgK*, which encodes an enzyme that catalyzes KDPG
460 production, resulted in significantly lower levels of replication at 10 h.p.i. compared to wild type;
461 this defect was rescued by complementation of *kdgK* at the native locus (**Fig. 5D**). These results
462 suggest that the ED pathway is important for the survival and replication of *S*. Tm by
463 compensating for nutrient limitation in the macrophage environment at later stages of infection.
464 More generally, these findings demonstrate the importance of profiling the dynamics of
465 transcriptional activity, particularly within changing conditions such as the intracellular
466 environment during infection.

Discussion

Fluorescence reporters are powerful tools for quantification of transcriptional dynamics at high temporal resolution, an especially relevant goal for bacteria like *S*. Tm that rapidly adapt their programming during environmental shifts. Capturing the dynamics across all stages of intracellular macrophage infection revealed a metabolic shift during the later stages of infection involving the ED pathway (**Fig. 5D**). Future investigations into the metabolic profile of intracellular *S*. Tm should involve integrating metabolic information from the host as well as the pathogen[67], including consideration of the time dependence of nutrient utilization. Mammalian cells employ multiple primary types of cellular metabolism. For example, when macrophages are activated in response to bacterial pathogens, they can undergo a shift from mitochondrial oxidative phosphorylation to aerobic glycolysis leading to depletion of intracellular glucose stores and the availability of oxygen, a typical terminal electron acceptor for aerobic metabolism in bacteria[15]. Importantly, these processes have been shown to be partly dependent on macrophage polarization status and need further exploration in this setting[71]. We propose that the host undergoes changes in metabolism that limit intracellular *S*. Tm replication through nutrient sequestration. In turn, *S*. Tm shifts its own metabolic programming at later stages of infection to overcome the glucose-limiting conditions in the SCV. This model is consistent with our findings wherein the ED pathway may provide alternate carbon sources to support *S.* Tm replication, although the replication defect of the Δ*kdgK* strain could also result from accumulation of toxic metabolic intermediates such as KDGP[72]. Taken altogether, our work provides further support for dynamic metabolic crosstalk between host and pathogen and motivates further exploration of the potential direct or indirect effects of ED pathway metabolic by-products on the host cell environment and immune responses.

Our library screens provided the first evidence of activity for many *S.* Tm genes, including some involved in pathogenicity (**Fig. 4B-F**). Previously published RNA-seq datasets catalogued

493 conditions under which many *S*. Tm genes are induced and identified TSS using dRNA-seq[12,13].
494 Our library and analyses complement these data sets by identifying activity from novel promoter
495 regions. Some of the novel promoter identifications result from our use of a genomic reference
496 with updated annotations and an unbiased computational approach to identify promoter regions.
497 Our ability to identify activity from some chromosomal regions whose expression was not detected
498 across 23 growth conditions using RNA-seq is likely to reflect our temporal approach that spanned
499 both growth and infection stages. Overall, our findings provide insight into the regulatory regions
500 of the *S*. Tm genome and highlight potential targets at different stages of infection for future drug
501 discovery focused on the inhibition of *S.* Tm pathogenesis.
502
503 Our comparative analysis among expression profiles during intracellular infection and controlled
504 *in vitro* growth highlights the power of our library to uncover the infection relevance of novel
505 promoter regions. In particular, our data sets revealed increased activity of several promoters
506 (e.g., P*mntR*, P*zur*, P*fur*) that regulate response of *S*. Tm to host nutritional immunity through
507 metal ion sequestration (**Fig. S10**). Our screens led to the hypothesis that *mntS* regulates the *S.*
508 Tm response to metal-limiting conditions in the SCV, and we found that P*mntS* activity was
509 dependent on environmental Mn^{2+} concentration *in vitro* (**Fig. 4E**). Because the activity of known
510 Mn^{2+} regulators, importers, and exporters lacked the sensitivity to Mn^{2+} concentration of P*mntS*,
511 we hypothesize that MntS plays a critical role in the ability of *S*. Tm to sense Mn^{2+} limitation in the
512 SCV (**Fig. 4E**). Moreover, our study highlights the remaining knowledge gap about *S.* Tm
513 adaptation during intracellular infection. Our candidate list of 234 novel promoters, many with
514 hypothetical or unknown functional annotations, and their quantified expression profiles should
515 provide compelling inspiration and a useful resource for future studies.
516
517 Our analyses also revealed that many prophage-associated promoters were activated during
518 infection (**Fig. 4F, S9**). One explanation for this activity is upregulation of genomic loci containing

519 phage-encoded virulence factors[50,51] (**Fig. 3F**). We also observed activity for other promoters of
520 prophage-associated genes, including ones involved in structural components and excision,
521 during the later stages of infection. This late-stage prophage promoter activity may be the result
522 of accumulation of DNA damage following ROS exposure during intracellular *S*. Tm replication
523 and the resulting SOS response, a known inducer of prophage loci[50,73–75]. While further
524 investigation is needed to elucidate whether host ROS production can lead to prophage induction,
525 these data may provide insight into other mechanisms of *Salmonella* survival during infection. For
526 example, in the intracellular pathogen *Listeria monocytogenes*, its DNA uptake competence
527 (Com) system is required during intracellular infection to promote escape from the macrophage
528 phagosome, and regulation of the Com system relies on prophage excision[76].
529
530 Promoter constructs have specific limitations for transcriptional profiling. For example, our
531 bioinformatic approach may not accurately capture the promoters for every coding region.
532 Additionally, some promoter regions that were expected to have high activity in SPI2-inducing
533 conditions (e.g., P*ssaM*) did not show activity either *in vitro* or during macrophage infection,
534 potentially due to the lack of key regulatory regions that lie >350 bp upstream of the TSS. In our
535 analyses, we focused on the large fraction of reporter strains that showed activity in at least one
536 condition, but false negative reporters could be used to investigate such regulation through further
537 strain construction (e.g., with larger upstream regions[77]). We opted to use a fast-folding and stable
538 GFP to accurately capture the first initiation of activity, hence GFP fluorescence signal does not
539 provide an accurate estimate of downregulation of promoter activity or translational regulation.
540 We note that the absence of complete repressor-binding sites could drive artificial promoter
541 activity. We discovered that SPI2-inducing *in vitro* conditions impose physiological defects during
542 stationary phase, and it is unclear whether such changes reflect conditions in the SCV. This work,
543 combined with other RNA-seq datasets, can be used to improve *in vitro* media conditions
544 designed to mimic aspects of the intra-macrophage environment.

Our bulk measurement approach to profiling transcriptional dynamics leaves outstanding questions about phenotypic heterogeneity. In this work, we demonstrate heterogeneous expression of SPI2 genes such as *ssaR* and *ssaG* (**Fig. 1G,H**). As expected, we also observed qualitative heterogeneity for SPI1 promoters during the early stages of macrophage invasion (**Fig. 3D**), and our library should serve as a powerful tool to expand our knowledge of which genes exhibit heterogenous expression and to understand how *S*. Tm regulates bistable expression during infection[47] using flow cytometry and high-throughput imaging[78]. By employing higher imaging resolution and improved single-cell segmentation, our library can be used to quantify the activity and heterogeneity of extracellular and intracellular bacteria during invasion of and replication in host cells (**Fig. 3D**)[79]. Moreover, our infection data only includes time points up to host cell lysis due to the increase in noise and inability to perform accurate image segmentation; nonetheless, our library provides future opportunities to profile and discover *S.* Tm gene regulation that occurs during host cell lysis and bacterial escape that could be important for pathogenesis.

Much remains to be discovered about *S.* Tm pathogenesis. The substantial set of genes whose expression has not yet been observed motivates screening across a more extensive and diverse collection of conditions to provide insight into gene functions. Our data can be used to inform time point selection for future RNA-seq or RT-qPCR experiments. Our library could also be used to infect different immune cell types or study the effects of various host-signaling factors to understand host-specific virulence programming. To probe *S.* Tm colonization throughout the gastrointestinal tract, the library could be screened *in vitro* in conditions that include bile, short chain fatty acids (SCFAs), gut-relevant carbon sources, and interactions with other gut commensals. To assist in the identification of therapies against *Salmonella* infections, future screens of the promoter library should include antibiotics, small molecules, and bacteriophages.

Our library of donor *E. coli* strains for high-throughput conjugation also enables straightforward plasmid transfer into other *Salmonella* strains or serovars. Collectively, our existing data and the future applications of our promoter libraries should provide a systems-level understanding of the timing of transcriptional programming during intracellular infection, with the potential to discover virulence mechanisms and treatments with global health impact.

Acknowledgements

We thank Marlin Jenkins (U. Minnesota) for providing the *S*. Tm SL1344::*phoN-dTomato* strain for library construction, Dirk Bumann (U. of Basel, Biozentrum) for providing the pFOK plasmid for site-specific mutagenesis, Sophie Helaine (Harvard Medical School) for providing the pFCcGi plasmid for quantifying bacterial replication, and Phoom Chairatana (Stanford) for providing guidance on plasmid construction. This study was funded in part by Award T32-AI007328-36 from the National Institute of General Medical Sciences (to O.R.D.), the Blavatnik Family Fellowship Fund (to O.R.D.), an NSF Graduate Research Fellowship (to T.H.N.), NSF Awards EF-2125383 and IOS-2032985 (to K.C.H.), NIH Awards R01 AI147023 and RM1 GM135102 (to K.C.H.), the Allen Discovery Center for Systems Modeling of Infection (to K.C.H., and D.M.M.), grants R01-AI116059 and R01-AI095396 from the National Institute of Allergy and Infectious Diseases (to D.M.M.), and Wellcome Trust Senior Investigator Award 222528/Z/21/Z (to J.C.D.H.). For the purpose of open access, the author has applied a CC BY public copyright license to any Author Accepted Manuscript version arising from this submission. The contents of this study are solely the responsibility of the authors and do not necessarily reflect the views of the Paul G. Allen Institute or the National Institutes of Health. The funders had no role in study design, data collection, and interpretation, or the decision to submit the work for publication.

Author Contributions

M.R., K.C.H., and D.M.M conceptualized research. T.H.N., O.R.D., D.M.M., and K.C.H. designed the research. M.R. performed computational identification of promoter regions. T.H.N., O.R.D., M.R., D.S.C.B., and B.X.W. performed the research. T.H.N. and O.R.D. analyzed the data. J.C.D.H. provided supervision. T.H.N., O.R.D., D.M.M., and K.C.H. wrote the paper, and all authors reviewed the manuscript prior to submission.

Declaration of Interests

602 The authors declare no competing interests.

Data and code availability

All data are available at https://purl.stanford.edu/fc012fq3845. Custom code used in this paper is available at https://doi.org/10.5281/zenodo.8339637. Any additional information required to reanalyze the data reported in this paper is available from the lead contact upon request.

Methods

Bacterial strains, macrophage cell lines, and growth conditions

Salmonella enterica serovar Typhimurium (*S*. Tm) strain SL1344 with *phoN-dTomato* integration (SL1344::*phoN-dTomato*) was used to construct the promoter library and for site-specific mutagenesis. *S.* Tm and *E. coli* strains used for conjugation are listed in **Table S1**. In preparation for screens, bacterial strains were grown overnight in selective media supplemented with 20 µg/mL chloramphenicol (Cm) and/or 50 µg/ml streptomycin (Strep) as required. For all intracellular infection studies, RAW 264.7 murine macrophages (ATCC #TIB-71) were maintained at 37 °C with 5% CO_2 in Dulbecco's Minimal Essential Medium (DMEM) (Invitrogen #11995073) supplemented with 10% Fetal Bovine Serum (Fisher Scientific #26-140-079).

Computational identification of promoter regions

2,907 lead-operon reporter regions were computationally identified based on open reading frames, intergenic regions, and experimentally validated transcriptional start sites[13] in the genome of *S.* Tm SL1344 (NCBI reference sequence NC_016810.1). Promoter regions were defined as the 350 bp upstream of and including the translational start site (353 bp total). Our library includes intergenic regions longer than 40 bp. The low-copy plasmid backbone pUA66[20] was used to construct the library with mGFPmut2[18], a Cm^R cassette, and *mob* genes for conjugative transfer from pSC101. For reporter plasmid constructs, each promoter was fused to *mGFPmut2* (including the S65A, V68L, S72A, and A206K mutations)[18]. Plasmids were assembled, sequence verified, and arrayed into 96-well plates by Thermo Fisher Scientific. All promoter sequences and respective well locations are available in **Table S2**, including promoter sequences that were not successfully cloned**.**

High-throughput plasmid transformation into E. coli

For each promoter plasmid, 50 µL of competent *E. coli* (MG1655 MFDpir RP4-2-Tc:[*Mu1*::*aac*(3)IV-Δ*aphA*-Δ*nic35* Δ*Mu2*::*zeo*] Δ*dapA*::(*erm-pir*) Δ*recA*) cells were mixed with ~10 ng of plasmid in one well of a 96-well PCR plate (Bio Rad #MLL9601). The mixtures were exposed to a cold shock via incubation on ice for 30 min, then heat shock in a 42 °C water bath for 45 s, followed by another cold shock on ice for 5 min. Cells were then added to 500 µL of fresh Lennox broth (LB, Fisher Scientific #50488761) containing 0.3 mM diammonium phosphate (DAP) in a deep-well 96-well plate (USA Scientific #1896-2110). Plates were sealed with breathable seals (Excel Scientific #LMT-AERAS-EX, T896100-S) and recovered for 1 h at 37 °C with shaking. To select for positive transformants through liquid selection, an additional 500 µL of LB containing 0.3 mM DAP and 40 µg/mL Cm (for a final Cm concentration of 20 µg/mL) were added and cells were grown overnight with shaking at 37 °C. In preparation for high-throughput conjugation, *E. coli* donor transformants were diluted 1:200 into fresh LB containing 0.3 mM DAP in 96-deepwell plates for another round of Cm (20 µg/mL) selection. After overnight growth with shaking at 37 °C, cultures were stored with 25% (v/v) glycerol at -80 °C in 96-well flat-bottom plates (Greiner Bio-One #655161) sealed with aluminum seals (Thermo Fisher Scientific #12-565-398).

High-throughput conjugation from* E. coli *to* S. *Tm

In preparation for high-throughput conjugation, an *E. coli* (donor) culture was grown under selection with 20 µg/mL Cm and a *S.* Tm (recipient) culture was grown under selection with 50 µg/mL Strep (natural resistance) overnight in LB with shaking at 37 °C. The overnight cultures were pelleted, washed, resuspended at 10X density, and mixed at a 1:4 (donor:recipient) ratio. Using a Benchsmart 96 semi-automatic pipetting system (Rainin), 5 µL of conjugation reactions were pipetted onto a rectangular LB-agar plate (Thermo Fisher Scientific #267060) containing 0.3 mM DAP and incubated at 37 °C for 5 h. Colonies were resuspended in LB and serially diluted on selective rectangular LB-agar plates (Thermo Fisher Scientific #264728) containing 20 µg/mL Cm and 50 µg/mL Strep without DAP to screen for positive *S*. Tm transformants and select against

E. coli donor cells, respectively. After overnight growth at 37 °C, single colonies were picked, grown to saturation at 37 °C in LB containing 20 µg/mL Cm and 50 µg/mL Strep, and stored with 25% glycerol at -80 °C in 96-well flat-bottom plates (Greiner Bio-One #655161).

Sequence verification of the promoter region in* S. *Tm strains

S. Tm strains were struck on LB-agar plates containing 20 µg/mL Cm and 50 µg/mL Strep and grown overnight at 37 °C. Colony PCR was performed by combining 25 µL of Accustart II 2x SuperMix (Quantabio #95137), 1 µL of 10 mM forward primer (PromLib_FWD 5′-AATAGGCGTATCACGAGG-3′), 1 µL of 10 mM reverse primer (PromLib_REV 5′-CCATCTAATTCAACAAGAATTGGG-3′), 18 µL of nuclease-free water, and 5 µL of a single colony diluted into 100 µL of nuclease-free water. The PCR program was 94 °C for 3 min, 35 cycles of [94 °C for 45 s, 50 °C for 60 s, and 72 °C for 90 s], followed by 72 °C for 10 min. Amplified products were confirmed by Sanger sequencing (Elim Bio).

In vitro *screening of the reporter library*

For *in vitro* screens, four media were used: NonSPI2 (SPI2 non-inducing), InSPI2 (SPI2 inducing), InSPI2 low Mg, and 10% BHI. Phosphate-carbon-nitrogen (PCN) base medium was used to make NonSPI2 (pH 7.4, 25 mM P_i, 1 mM $MgSO_4$), InSPI2 (pH 5.8, 0.4 mM Pi, 1 mM $MgSO_4$), and InSPI2 low magnesium (pH 5.8, 0.4 mM Pi, 10 µM $MgSO_4$)[12,28]. 10% Brain Heart Infusion (BHI, BD #2237500) medium was 100% BHI diluted in M9 salts (Sigma-Aldrich #M9956) and supplemented with 0.1 mM $CaCl_2$ and 2 mM $MgSO_4$; 10% BHI was used instead of 100% BHI to reduce background autofluorescence and thereby improve the dynamic range of GFP measurements. More details about media conditions can be found in **Table S5,6**. *S.* Tm glycerol stocks were pinned on selective rectangular LB plates (Thermo Fisher Scientific #267060) containing 20 µg/mL Cm and 50 µg/mL Strep. After overnight growth at 37 °C, colonies were picked and grown overnight at 37 °C in 200 µL of NonSPI2 or 10% BHI medium containing 20 µg/mL Cm and 50

685 µg/mL Strep in flat-bottom 96-well plates (Greiner Bio-One #655161) sealed with breathable seals
686 (Excel Scientific #LMT-AERAS-EX, T896100-S). Using a Benchsmart 96 semi-automatic
687 pipetting system (Rainin), overnight cultures were diluted 1:100 in 80 µL of the appropriate
688 medium (NonSPI2 into NonSPI2, InSPI2, or InSPI2 low Mg, or 10% BHI into 10% BHI) in black-
689 walled, clear-bottom 384-well plates (Greiner Bio #781097). Plates were sealed using transparent
690 seals (Excel Scientific #STR-SEAL-PLT) with small, laser-cut holes (~0.5 mm) for gas exchange.
691 Growth curves were measured using a Biotek Synergy H1 with continuous shaking at 37 °C for
692 24 h, during which OD_{600} and GFP (488 nm/520 nm excitation/emission) were measured every
693 10 min.
694
695 **In vitro screening *data analysis***
696 To quantify promoter expression, the GFP signal of the parent strain (no plasmid control) was
697 subtracted to correct for background fluorescence. To normalize for cell number, the parent-
698 subtracted GFP signal was normalized by OD_{600} after subtracting the background absorbance of
699 a blank well (no cells). In all analyses, the denominator was set to a minimum value of 0.3 to avoid
700 fluctuations resulting from division by small values. A promoter was classified as ON if its
701 expression was at least two standard deviations above a dynamic estimate of background noise
702 for at least 3 timepoints (30 min) (**Fig. S2**). Background noise was estimated by calculating the
703 mean over a time interval t^* of n^* of the lowest-expressing promoters that could be safely assumed
704 to be OFF in the medium of interest. For each medium, t^* was identified as the time range starting
705 when OD_{600} reached 0.3 and ending when promoter activity was still detectable in each condition
706 to avoid the physiological complications of late stationary phase in InSPI2 and InSPI2 low Mg.
707 Therefore, t^* was identified for NonSPI2 as 8–24 h, 8–16 h for InSPI2, 8–16 h for InSPI2 low Mg,
708 and 4–24 h for 10% BHI. To calculate n^*, the expression dynamics of the n lowest-expressing
709 promoters were averaged for a range of values of n, using only data within t^*. Finally, the value
710 of n^* was selected based on the mean trajectory being closest to 0. All data analyses were

711 performed in R with custom scripts, using packages *dplyr*, *genefilter*, *ggExtra*, *ggplot2*, *gridExtra*,
712 *numbers*, *numDeriv*, *pheatmap*, *Rcolorbrewer*, *realxl*, *svglite*, *tidyverse*, *VennDiagram*, and *zoo*.
713 All data are available at https://purl.stanford.edu/fc012fq3845. All custom scripts are available at
714 https://doi.org/10.5281/zenodo.8339637.
715
716 ***Single-cell fluorescence imaging and analysis***
717 Single colonies of reporter and parental strains were inoculated into 200 µL of NonSPI2 medium.
718 After overnight growth at 37 °C, saturated cultures were diluted 1:100 into 200 µL of fresh
719 NonSPI2, InSPI2, and InSPI2 low Mg media and were grown with shaking at 37 °C. To aid in
720 image segmentation, all cultures were diluted 1:5 in PBS at 8 h, and 1:20, 1:10, and none for
721 NonSPI2, InSPI2, and InSPI2 low Mg, respectively, at 24 h. For imaging, 1 µL of cells was spotted
722 on a 1.5% PBS-agarose pad and allowed to dry before sealing with a coverslip. Phase-contrast
723 images were acquired with a Ti-E inverted microscope (Nikon Instruments) using a 100X (NA:
724 1.40) oil immersion objective and a Neo 5.5 sCMOS camera (Andor Technology). Images were
725 acquired using µManager v. 2.0. To calculate GFP intensity per cell, the MATLAB image
726 processing package *Morphometrics*[80] was used to segment cells from phase-contrast images.
727 Images were filtered for single-cell contours. For each of >1,000 contours in each condition, the
728 median background-subtracted GFP fluorescence was calculated for each cell. Phase-contrast
729 and GFP images were overlaid in FIJI. All data analysis was performed with custom MATLAB
730 scripts. All data are available at https://purl.stanford.edu/fc012fq3845. All custom scripts are
731 available at https://doi.org/10.5281/zenodo.8339637.
732
733 ***pH measurements during* in vitro *growth***
734 A single colony of the parent strain was inoculated into 5 mL of NonSPI2 containing 50 µg/mL
735 Strep and grown overnight with shaking at 37 °C. Overnight cultures were diluted 1:100 into 5 mL
736 of fresh NonSPI2, InSPI2, or InSPI2 low Mg in three technical replicates. After 24 h of growth,

737 cultures were centrifuged at 4,000*g* for 10 min and filter sterilized with 0.22-µm filters. The pH of
738 NonSPI2, InSPI2, and InSPI2 low Mg cultures before and after 24 h of *S.* Tm growth was
739 measured using a pH probe (Thermo Fisher Scientific #13-620).
740
741 ***Intracellular screening in macrophages***
742 To characterize transcriptional responses of *S.* Tm during infection, we performed high-
743 throughput, time-lapse fluorescence microscopy in RAW 264.7 murine macrophages. For
744 infection, macrophages were seeded in black-walled, clear-bottom 96-well plates (Corning #3603)
745 at ~10^4 cells per well. *S.* Tm glycerol stocks were pinned onto selective rectangular LB-agar plates
746 (Thermo Fisher Scientific #267060) containing 20 µg/mL Cm and 50 µg/mL Strep. After overnight
747 growth at 37 °C, colonies were picked into 500 µL of LB with 20 µg/mL Cm and 50 µg/mL Strep
748 in round-bottom, 96-well deep-well plates (VWR #76210-518), sealed with breathable seals (USA
749 Scientific #9126-2100), and grown for 16 h at 37 °C. *S.* Tm cultures were washed in PBS
750 (Invitrogen #10010-049) and resuspended in FlouroBrite DMEM (FDMEM, ThermoFisher
751 #A1896701) supplemented with 7% Fetal Bovine Serum, 10 mM HEPES (Gibco #15630-080), 2
752 mM L-glutamine (Thermo #25030081), and 500 µg/mL L-histidine (Sigma #H6034-25G).
753 Macrophages were infected for 40 min at a multiplicity of infection of 10:1 (bacteria:macrophages)
754 and centrifuged at 250*g* for 5 min. Following the invasion period, cultures were maintained in
755 FDMEM supplemented with 100 µg/mL gentamicin for 50 min to kill extracellular bacteria. Infected
756 macrophages were washed with PBS and maintained in FDMEM supplemented with 15 µg/mL
757 gentamicin for 24 h post infection. Plates of infected macrophages were imaged in triplicate per
758 well in an Incucyte S3 Live-Cell Analysis Platform (Sartorius #4647). Phase and fluorescence
759 images were collected every hour per well using a 20X objective. Fluorescence images were
760 acquired using red (excitation: 565-605 nm, emission: 625-705 nm) and green (excitation: 440-
761 480 nm, emission: 504-544 nm) channels.
762

763 ***Macrophage infection image analysis***

764 Fluorescence background subtraction was performed using the IncuCyte Surface Fit algorithm
765 and cell outlines were segmented using the Cell-by-cell analysis software (Sartorius #9600-0031).
766 After segmentation, cells were classified into GFP OFF/ON and dTomato OFF/ON according to
767 fluorescence intensity thresholds (GFP: 0.0853 arbitrary fluorescence units (AFU), dTomato:
768 0.0309 AFU). At each time point between 1–4 h.p.i., promoter activity was quantified as the
769 difference between the mean GFP fluorescence for GFP-positive macrophages infected by the
770 strain of interest and the mean GFP fluorescence for all macrophages of the parent strain without
771 a plasmid to correct for background and fluorescence bleed-through. At each time point between
772 5–15 h.p.i., promoter activity was quantified as the difference between the mean GFP
773 fluorescence for dTomato-positive macrophages infected by the strain of interest and the mean
774 GFP fluorescence for all macrophages of the parent strain without a plasmid to correct for
775 background and fluorescence bleed-through. To normalize for bacterial cell number, the
776 background-subtracted GFP signal was normalized by the dTomato signal of the promoter strain
777 after subtraction of the background dTomato signal of a separate well seeded with uninfected
778 macrophages. In all analyses, minimum values of 0.005 AFU and 0.04 AFU were used for the
779 GFP and dTomato signals, respectively, to avoid fluctuations resulting from division by small
780 values. Following normalization, fluorescence signal is reported as relative fluorescence units
781 (RFU). A dynamic estimate of background noise for each time window was determined as the
782 mean GFP signal from GFP- (1–4 h.p.i.) or dTomato-positive (5–15 h.p.i.) macrophages infected
783 with the parent strain for each time point. A promoter was classified as active if the GFP signal
784 was at least two standard deviations above a dynamic estimate of background noise for a given
785 time window (**Fig. S6**). All data analyses were performed in R using custom scripts. All data are
786 available at https://purl.stanford.edu/fc012fq3845. All custom scripts are available at
787 https://doi.org/10.5281/zenodo.8339637.
788

Functional annotations

Functional annotations were obtained for the *S.* Typhimurium LT2 reference genome, leveraging existing Gene Ontology (GO) terms for biological processes and molecular functions that were exported from BioCyc. These annotations were subsequently mapped to the *S.* Typhimurium SL1344 genome through ortholog mapping. To streamline genome-wide functional annotations, BioCyc-based annotations were subjected to manual curation, resulting in a total of 91 categories (**Table S2**). Unnamed genes with no recorded GO terms were designated as hypothetical genes. Subsequently, the functional category for each promoter designated as ON in the dataset was recorded to quantify the number of promoters belonging to each functional class.

S. *Tm mutant strain construction*

For clean site-specific mutagenesis, a dual-negative selection-based approach was used as previously described[81]. All strains, primers, and plasmids used for *S*. Tm strain construction are listed in **Table S1**. All plasmid constructs were cloned into *E. coli* DH5α or the DAP-dependent donor strain JKe201[82]. For deletion of *kdgT*, *kdgK*, *edd*, *eda*, *uxuA*, and *idnK*, four primers were used to amplify ~1 kb upstream and downstream of the given gene and the amplicons were Gibson assembled into the pFOK suicide vector. This construct results in a scarless deletion and the resulting plasmids were confirmed via Sanger sequencing and then transformed into *E*. *coli* DH5α/JKe201. Plasmids were conjugated into wild-type *S*. Tm SL1344 and selected by kanamycin resistance. Stable deletion from the *S*. Tm SL1344 genome required two consecutive homologous recombination events on 20% sucrose with 0.5 µg/mL anhydrous tetracycline (AHT) plates. Two markers were used for negative selection against merodiploids that still have the plasmid integrated into the backbone, using a tetracycline-inducible P_{tet} promoter controlling the expression of *sacB* and *I-sceI*. Surviving colonies contained the clean deletion of a given gene and were sequence verified using the appropriate primers (**Table S1**).

Replication rate measurements during macrophage infection

Approximately 10^6 RAW 264.7 cells were seeded into 12-well plates (Fisher scientific #08-772-29) and grown overnight for half a doubling. Wild-type and mutant *S.* Tm strains containing the pFccGi reporter plasmid, which encodes mCherry under constitutive expression and GFP under arabinose-inducible expression, were grown overnight in LB with 2% arabinose and appropriate antibiotics. The next day, cells were washed and infected using the protocol described above. Cells were processed at 2, 6, and 10 h.p.i. for flow cytometry. Cells were washed and harvested in flow wash buffer (2% FBS, 0.1% ethylenediaminetetraacetic acid (EDTA) in PBS), stained with LIVE/DEAD stain for 15 min (Thermo Fisher scientific #L34966), fixed and permeabilized for 15 min using Cytofix/Cytoperm (BD Biosciences #554714), washed in permeabilization/wash buffer (BD Biosciences #554714), and resuspended in flow wash buffer. Cells were counted on a Cytek Aurora flow cytometer and analyzed using FlowJo. Live cells were gated based on positive mCherry signal and fold replication was determined using the ratio of the mean GFP and mean mCherry signal from mCherry-positive cells[69].

References

1. Gal-Mor, O., Boyle, E. C. & Grassl, G. A. Same species, different diseases: how and why typhoidal and non-typhoidal Salmonella enterica serovars differ. *Front Microbiol* **5**, 391 (2014).
2. Kirk, M. D. *et al.* World Health Organization Estimates of the Global and Regional Disease Burden of 22 Foodborne Bacterial, Protozoal, and Viral Diseases, 2010: A Data Synthesis. *PLoS Med* **12**, e1001921 (2015).
3. Castro-Vargas, R. E., Herrera-Sánchez, M. P., Rodríguez-Hernández, R. & Rondón-Barragán, I. S. Antibiotic resistance in Salmonella spp. isolated from poultry: A global overview. *Vet World* **13**, 2070–2084 (2020).
4. Parisi, A. *et al.* Health Outcomes from Multidrug-Resistant *Salmonella* Infections in High-Income Countries: A Systematic Review and Meta-Analysis. *Foodborne Pathogens and Disease* **15**, 428–436 (2018).
5. Wang, X. *et al.* Antibiotic Resistance in Salmonella Typhimurium Isolates Recovered From the Food Chain Through National Antimicrobial Resistance Monitoring System Between 1996 and 2016. *Front. Microbiol.* **10**, 985 (2019).
6. Xiang, Y. *et al.* Investigation of a Salmonellosis Outbreak Caused by Multidrug Resistant Salmonella Typhimurium in China. *Front. Microbiol.* **11**, 801 (2020).
7. Petersen, E. & Miller, S. I. The cellular microbiology of Salmonellae interactions with macrophages. *Cellular Microbiology* **21**, e13116 (2019).
8. Steele-Mortimer, O. The Salmonella-containing vacuole—Moving with the times. *Current Opinion in Microbiology* **11**, 38–45 (2008).
9. Lou, L., Zhang, P., Piao, R. & Wang, Y. Salmonella Pathogenicity Island 1 (SPI-1) and Its Complex Regulatory Network. *Front. Cell. Infect. Microbiol.* **9**, 270 (2019).

10. Pillay, T. D. *et al.* Speaking the host language: how Salmonella effector proteins manipulate the host: This article is part of the Bacterial Cell Envelopes collection. *Microbiology* **169**, (2023).
11. Eriksson, S., Lucchini, S., Thompson, A., Rhen, M. & Hinton, J. C. D. Unravelling the biology of macrophage infection by gene expression profiling of intracellular Salmonella enterica: Global gene expression profiling of intracellular Salmonella. *Molecular Microbiology* **47**, 103–118 (2002).
12. Kröger, C. *et al.* An Infection-Relevant Transcriptomic Compendium for Salmonella enterica Serovar Typhimurium. *Cell Host & Microbe* **14**, 683–695 (2013).
13. Srikumar, S. *et al.* RNA-seq Brings New Insights to the Intra-Macrophage Transcriptome of Salmonella Typhimurium. *PLoS Pathog* **11**, e1005262 (2015).
14. Avital, G. *et al.* scDual-Seq: mapping the gene regulatory program of Salmonella infection by host and pathogen single-cell RNA-sequencing. *Genome Biol* **18**, 200 (2017).
15. Rosenberg, G., Riquelme, S., Prince, A. & Avraham, R. Immunometabolic crosstalk during bacterial infection. *Nat Microbiol* **7**, 497–507 (2022).
16. Rolfe, M. D. *et al.* Lag phase is a distinct growth phase that prepares bacteria for exponential growth and involves transient metal accumulation. *J Bacteriol* **194**, 686–701 (2012).
17. Jenniches, L. *et al.* Improved RNA stability estimation through Bayesian modeling reveals most bacterial transcripts have sub-minute half-lives. 2023.06.15.545072 Preprint at https://doi.org/10.1101/2023.06.15.545072 (2023).
18. Balleza, E., Kim, J. M. & Cluzel, P. Systematic characterization of maturation time of fluorescent proteins in living cells. *Nat Methods* **15**, 47–51 (2018).
19. Silander, O. K. *et al.* A Genome-Wide Analysis of Promoter-Mediated Phenotypic Noise in Escherichia coli. *PLoS Genet* **8**, e1002443 (2012).

878 20. Zaslaver, A. *et al.* A comprehensive library of fluorescent transcriptional reporters for
879 Escherichia coli. *Nat Methods* **3**, 623–628 (2006).
880 21. Diacovich, L., Lorenzi, L., Tomassetti, M., Méresse, S. & Gramajo, H. The infectious
881 intracellular lifestyle of *Salmonella enterica* relies on the adaptation to nutritional conditions
882 within the *Salmonella* -containing vacuole. *Virulence* **8**, 975–992 (2017).
883 22. Robijns, S. C. A. *et al.* A GFP promoter fusion library for the study of *Salmonella* biofilm
884 formation and the mode of action of biofilm inhibitors. *Biofouling* **30**, 605–625 (2014).
885 23. Schulte, M., Olschewski, K. & Hensel, M. Fluorescent protein-based reporters reveal stress
886 response of intracellular Salmonella enterica at level of single bacterial cells. *Cellular*
887 *Microbiology* **23**, e13293 (2021).
888 24. Ferrières, L. *et al.* Silent Mischief: Bacteriophage Mu Insertions Contaminate Products of
889 Escherichia coli Random Mutagenesis Performed Using Suicidal Transposon Delivery
890 Plasmids Mobilized by Broad-Host-Range RP4 Conjugative Machinery. *J Bacteriol* **192**,
891 6418–6427 (2010).
892 25. Barat, S. *et al.* Immunity to Intracellular Salmonella Depends on Surface-associated
893 Antigens. *PLoS Pathog* **8**, e1002966 (2012).
894 26. Goldberg, M. F. *et al.* Salmonella Persist in Activated Macrophages in T Cell-Sparse
895 Granulomas but Are Contained by Surrounding CXCR3 Ligand-Positioned Th1 Cells.
896 *Immunity* **49**, 1090-1102.e7 (2018).
897 27. Kasahara, M., Nakata, A. & Shinagawa, H. Molecular analysis of the Salmonella
898 typhimurium phoN gene, which encodes nonspecific acid phosphatase. *J. Bacteriol.* **173**,
899 6760–6765 (1991).
900 28. Löber, S., Jäckel, D., Kaiser, N. & Hensel, M. Regulation of Salmonella pathogenicity island
901 2 genes by independent environmental signals. *International Journal of Medical*
902 *Microbiology* **296**, 435–447 (2006).

29. Aranda-Díaz, A. *et al.* Establishment and characterization of stable, diverse, fecal-derived in vitro microbial communities that model the intestinal microbiota. *Cell Host & Microbe* **30**, 260-272.e5 (2022).
30. Halsey, T. A., Vazquez-Torres, A., Gravdahl, D. J., Fang, F. C. & Libby, S. J. The Ferritin-Like Dps Protein Is Required for Salmonella enterica Serovar Typhimurium Oxidative Stress Resistance and Virulence. *Infect Immun* **72**, 1155–1158 (2004).
31. Wong, V. K. *et al.* Characterization of the yehUT Two-Component Regulatory System of Salmonella enterica Serovar Typhi and Typhimurium. *PLOS ONE* **8**, e84567 (2013).
32. Fass, E. & Groisman, E. A. Control of Salmonella pathogenicity island-2 gene expression. *Curr Opin Microbiol* **12**, 199–204 (2009).
33. Tsai, C. N. & Coombes, B. K. The Role of the Host in Driving Phenotypic Heterogeneity in Salmonella. *Trends in Microbiology* **27**, 508–523 (2019).
34. Helaine, S. *et al.* Internalization of *Salmonella* by Macrophages Induces Formation of Nonreplicating Persisters. *Science* **343**, 204–208 (2014).
35. Sutterlin, H. A. *et al.* Disruption of lipid homeostasis in the Gram-negative cell envelope activates a novel cell death pathway. *Proceedings of the National Academy of Sciences* **113**, E1565–E1574 (2016).
36. Rojas, E. R. *et al.* The outer membrane is an essential load-bearing element in Gram-negative bacteria. *Nature* **559**, 617–621 (2018).
37. Soncini, F. C., García Véscovi, E., Solomon, F. & Groisman, E. A. Molecular basis of the magnesium deprivation response in Salmonella typhimurium: identification of PhoP-regulated genes. *Journal of Bacteriology* **178**, 5092–5099 (1996).
38. Bauer, K., Benz, R., Brass, J. & Boos, W. Salmonella typhimurium contains an anion-selective outer membrane porin induced by phosphate starvation. *Journal of Bacteriology* **161**, 813–816 (1985).

928 39. Osborne, S. E. & Coombes, B. K. Transcriptional Priming of Salmonella Pathogenicity
929 Island-2 Precedes Cellular Invasion. *PLoS ONE* **6**, e21648 (2011).
930 40. van der Heijden, J., Bosman, E. S., Reynolds, L. A. & Finlay, B. B. Direct measurement of
931 oxidative and nitrosative stress dynamics in Salmonella inside macrophages. *Proceedings*
932 *of the National Academy of Sciences* **112**, 560–565 (2015).
933 41. Powers, T. R. *et al.* Intracellular niche-specific profiling reveals transcriptional adaptations
934 required for the cytosolic lifestyle of Salmonella enterica. *PLOS Pathogens* **17**, e1009280
935 (2021).
936 42. Lou, L., Zhang, P., Piao, R. & Wang, Y. Salmonella Pathogenicity Island 1 (SPI-1) and Its
937 Complex Regulatory Network. *Front. Cell. Infect. Microbiol.* **9**, 270 (2019).
938 43. Cirillo, D. M., Valdivia, R. H., Monack, D. M. & Falkow, S. Macrophage-dependent induction
939 of the Salmonella pathogenicity island 2 type III secretion system and its role in intracellular
940 survival. *Molecular Microbiology* **30**, 175–188 (1998).
941 44. Ellermeier, C. D., Ellermeier, J. R. & Slauch, J. M. HilD, HilC and RtsA constitute a feed
942 forward loop that controls expression of the SPI1 type three secretion system regulator hilA
943 in Salmonella enterica serovar Typhimurium. *Molecular Microbiology* **57**, 691–705 (2005).
944 45. Rakeman, J. L., Bonifield, H. R. & Miller, S. I. A HilA-Independent Pathway to Salmonella
945 typhimurium Invasion Gene Transcription. *Journal of Bacteriology* **181**, 3096–3104 (1999).
946 46. Hautefort, I., Proença, M. J. & Hinton, J. C. D. Single-Copy Green Fluorescent Protein Gene
947 Fusions Allow Accurate Measurement of Salmonella Gene Expression In Vitro and during
948 Infection of Mammalian Cells. *Applied and Environmental Microbiology* **69**, 7480–7491
949 (2003).
950 47. Sánchez-Romero, M. A. & Casadesús, J. Single Cell Analysis of Bistable Expression of
951 Pathogenicity Island 1 and the Flagellar Regulon in Salmonella enterica. *Microorganisms* **9**,
952 210 (2021).

953 48. Knuff, K. & Finlay, B. B. What the SIF Is Happening—The Role of Intracellular Salmonella-
954 Induced Filaments. *Front. Cell. Infect. Microbiol.* **7**, 335 (2017).
955 49. Beuzon, C. R. Salmonella maintains the integrity of its intracellular vacuole through the
956 action of SifA. *The EMBO Journal* **19**, 3235–3249 (2000).
957 50. Wahl, A., Battesti, A. & Ansaldi, M. Prophages in Salmonella enterica: a driving force in
958 reshaping the genome and physiology of their bacterial host? *Mol Microbiol* **111**, 303–316
959 (2019).
960 51. Ho, T. D. *et al.* Identification of GtgE, a Novel Virulence Factor Encoded on the Gifsy-2
961 Bacteriophage of Salmonella enterica Serovar Typhimurium. *J Bacteriol* **184**, 5234–5239
962 (2002).
963 52. Wright, J. A. *et al.* Multiple redundant stress resistance mechanisms are induced in
964 Salmonella enterica serovar Typhimurium in response to alteration of the intracellular
965 environment via TLR4 signalling. *Microbiology* **155**, 2919–2929 (2009).
966 53. Rowley, G., Spector, M., Kormanec, J. & Roberts, M. Pushing the envelope:
967 extracytoplasmic stress responses in bacterial pathogens. *Nat Rev Microbiol* **4**, 383–394
968 (2006).
969 54. Humphreys, S., Stevenson, A., Bacon, A., Weinhardt, A. B. & Roberts, M. The Alternative
970 Sigma Factor, ςE, Is Critically Important for the Virulence of Salmonella typhimurium.
971 *Infection and Immunity* **67**, 1560–1568 (1999).
972 55. Riva, R., Korhonen, T. K. & Meri, S. The outer membrane protease PgtE of Salmonella
973 enterica interferes with the alternative complement pathway by cleaving factors B and H.
974 *Frontiers in Microbiology* **6**, (2015).
975 56. Brewer, S. M., Brubaker, S. W. & Monack, D. M. Host inflammasome defense mechanisms
976 and bacterial pathogen evasion strategies. *Current Opinion in Immunology* **60**, 63–70
977 (2019).

978 57. Gibson, D. L. *et al.* Salmonella Produces an O-Antigen Capsule Regulated by AgfD and
979 Important for Environmental Persistence. *J Bacteriol* **188**, 7722–7730 (2006).
980 58. Ruddle, S. J., Massis, L. M., Cutter, A. C. & Monack, D. M. Salmonella-liberated dietary L-
981 arabinose promotes expansion in superspreaders. *Cell Host & Microbe* **31**, 405-417.e5
982 (2023).
983 59. Rolfe, M. D. *et al.* Lag Phase Is a Distinct Growth Phase That Prepares Bacteria for
984 Exponential Growth and Involves Transient Metal Accumulation. *Journal of Bacteriology*
985 **194**, 686–701 (2012).
986 60. Westermann, A. J. *et al.* Dual RNA-seq unveils noncoding RNA functions in host–pathogen
987 interactions. *Nature* **529**, 496–501 (2016).
988 61. Waters, L. S., Sandoval, M. & Storz, G. The Escherichia coli MntR Miniregulon Includes
989 Genes Encoding a Small Protein and an Efflux Pump Required for Manganese
990 Homeostasis. *Journal of Bacteriology* **193**, 5887–5897 (2011).
991 62. Martin, J. E., Waters, L. S., Storz, G. & Imlay, J. A. The Escherichia coli Small Protein MntS
992 and Exporter MntP Optimize the Intracellular Concentration of Manganese. *PLOS Genetics*
993 **11**, e1004977 (2015).
994 63. Uppalapati, S. R. & Vazquez-Torres, A. Manganese Utilization in Salmonella Pathogenesis:
995 Beyond the Canonical Antioxidant Response. *Front Cell Dev Biol* **10**, 924925 (2022).
996 64. Ouyang, A., Gasner, K. M., Neville, S. L., McDevitt, C. A. & Frawley, E. R. MntP and YiiP
997 Contribute to Manganese Efflux in Salmonella enterica Serovar Typhimurium under
998 Conditions of Manganese Overload and Nitrosative Stress. *Microbiology Spectrum* **10**,
999 e01316-21 (2022).
1000 65. Jeon, Y. *et al.* Development of novel Escherichia coli cell-based biosensors to monitor
1001 Mn(II) in environmental systems. *Frontiers in Microbiology* **13**, (2022).
1002 66. Kelley, L. A., Mezulis, S., Yates, C. M., Wass, M. N. & Sternberg, M. J. E. The Phyre2 web
1003 portal for protein modeling, prediction and analysis. *Nat Protoc* **10**, 845–858 (2015).

67. Mitosch, K. *et al.* A pathogen-specific isotope tracing approach reveals metabolic activities and fluxes of intracellular Salmonella. *PLOS Biology* **21**, e3002198 (2023).

68. Peekhaus, N. & Conway, T. What's for Dinner?: Entner-Doudoroff Metabolism in *Escherichia coli*. *J Bacteriol* **180**, 3495–3502 (1998).

69. Figueira, R., Watson, K. G., Holden, D. W. & Helaine, S. Identification of Salmonella Pathogenicity Island-2 Type III Secretion System Effectors Involved in Intramacrophage Replication of S. enterica Serovar Typhimurium: Implications for Rational Vaccine Design. *mBio* **4**, e00065-13 (2013).

70. Figueira, R., Watson, K. G., Holden, D. W. & Helaine, S. Identification of Salmonella Pathogenicity Island-2 Type III Secretion System Effectors Involved in Intramacrophage Replication of S. enterica Serovar Typhimurium: Implications for Rational Vaccine Design. *mBio* **4**, 10.1128/mbio.00065-13 (2013).

71. Thiriot, J. D., Martinez-Martinez, Y. B., Endsley, J. J. & Torres, A. G. Hacking the host: exploitation of macrophage polarization by intracellular bacterial pathogens. *Pathogens and Disease* **78**, ftaa009 (2020).

72. Fuhrman, L. K., Wanken, A., Nickerson, K. W. & Conway, T. Rapid accumulation of intracellular 2-keto-3-deoxy-6-phosphogluconate in an Entner-Doudoroff aldolase mutant results in bacteriostasis. *FEMS Microbiology Letters* **159**, 261–266 (1998).

73. Garcia-Russell, N., Elrod, B. & Dominguez, K. Stress-induced prophage DNA replication in Salmonella enterica serovar Typhimurium. *Infection, Genetics and Evolution* **9**, 889–895 (2009).

74. Michaux, C., Ronneau, S., Giorgio, R. T. & Helaine, S. Antibiotic tolerance and persistence have distinct fitness trade-offs. *PLoS Pathog* **18**, e1010963 (2022).

75. Bodner, K. *et al.* Engineered Fluorescent E. coli Lysogens Allow Live-Cell Imaging of Functional Prophage Induction Triggered inside Macrophages. *Cell Systems* **10**, 254-264.e9 (2020).

76. Rabinovich, L., Sigal, N., Borovok, I., Nir-Paz, R. & Herskovits, A. A. Prophage Excision Activates Listeria Competence Genes that Promote Phagosomal Escape and Virulence. *Cell* **150**, 792–802 (2012).

77. Collado-Vides, J. *et al.* Bioinformatics Resources for the Study of Gene Regulation in Bacteria. *J Bacteriol* **191**, 23–31 (2009).

78. Shi, H., Colavin, A., Lee, T. K. & Huang, K. C. Strain Library Imaging Protocol for high-throughput, automated single-cell microscopy of large bacterial collections arrayed on multiwell plates. *Nat Protoc* **12**, 429–438 (2017).

79. Van Valen, D. A. *et al.* Deep Learning Automates the Quantitative Analysis of Individual Cells in Live-Cell Imaging Experiments. *PLoS Comput Biol* **12**, e1005177 (2016).

80. Ursell, T. *et al.* Rapid, precise quantification of bacterial cellular dimensions across a genomic-scale knockout library. *BMC Biology* **15**, 17 (2017).

81. Cianfanelli, F. R., Cunrath, O. & Bumann, D. Efficient dual-negative selection for bacterial genome editing. *BMC Microbiol* **20**, 129 (2020).

82. Harms, A. *et al.* A bacterial toxin-antitoxin module is the origin of inter-bacterial and inter-kingdom effectors of Bartonella. *PLoS Genet* **13**, e1007077 (2017).

Figures

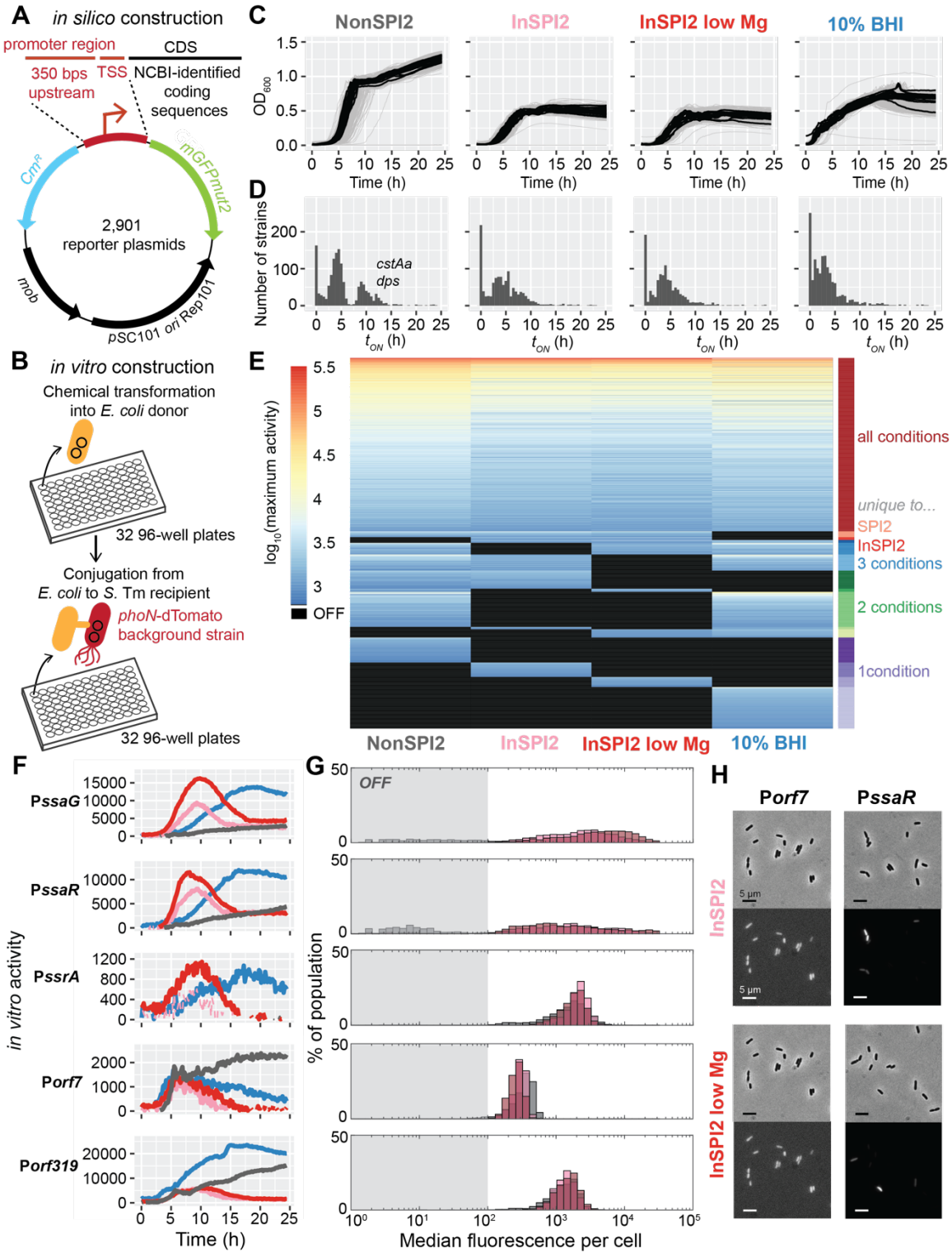

Figure 1: High-throughput construction of a comprehensive *S.* Tm reporter library enables activity profiling across *in vitro* media conditions.

A) Plasmid map of the reporter-GFP fusions in the library. Promoter regions were identified as the 350 bp upstream of and including the TSS, followed by the *mGFPmut2* sequence, the pSC101 origin of replication, the *mob* mobilization region for conjugative transfer, and a chloramphenicol (Cm)-resistance (Cm^R) cassette.

B) High-throughput cloning strategy used to generate the library. Plasmids were chemically transformed into *E. coli*, and positive transformants were used for conjugation into a *S.* Tm parental strain with *dTomato* integrated at the *phoN* locus. Positive *E. coli* and *S.* Tm transformants are stored in 32 96-well plates.

C) Background-subtracted optical density (OD_{600}) dynamics for all reporter strains in four *in vitro* media conditions (NonSPI2, InSPI2, InSPI2 low Mg, and 10% BHI). Growth curves for reporter strains are shown in gray, and background (promoter-less) strains are shown as thick black lines.

D) Histograms of the time t_{ON} at which reporters first exhibited significant activity in each medium (NonSPI2, InSPI2, InSPI2 low Mg, and 10% BHI).

E) Maximum activity for the 1,850 reporters that turned ON in at least one *in vitro* condition. Activity is reported as parent-subtracted GFP normalized by background-subtracted OD_{600}. Reporters are ordered by their shared activity across media. Black values denote OFF activity.

F) Promoter activity dynamics for five SPI2 operon reporters (*ssaG*, *ssaR*, *ssrA*, *orf7*, *orf319*) in NonSPI2 (grey), InSPI2 (pink), InSPI2 low Mg (red), and 10% BHI (blue). Activity is reported as GFP (parent-subtracted to account for autofluorescence) normalized to blanked OD_{600} (to account for changes in cell number). A promoter was defined as ON based on comparison to a dynamic estimate of background noise (**Methods**). ON activity is denoted by solid lines, whereas OFF activity is denoted by dashed lines.

G) Histograms of median GFP intensity for >1,000 cells in NonSPI2 (grey), InSPI2 (pink), and InSPI2 Low Mg (red) for the strains in (F). P*ssaG* and P*ssaR* cells exhibited substantial fluorescence heterogeneity. Strains were imaged after 8 h of growth in each medium.

H) Representative phase (left) and GFP (right) images of P*orf7* and P*ssaR* cells after 8 h of growth in InSPI2 and InSPI2 low Mg. Fluorescence contrast was adjusted for each strain to highlight population heterogeneity. Scale bar: 5 μm.

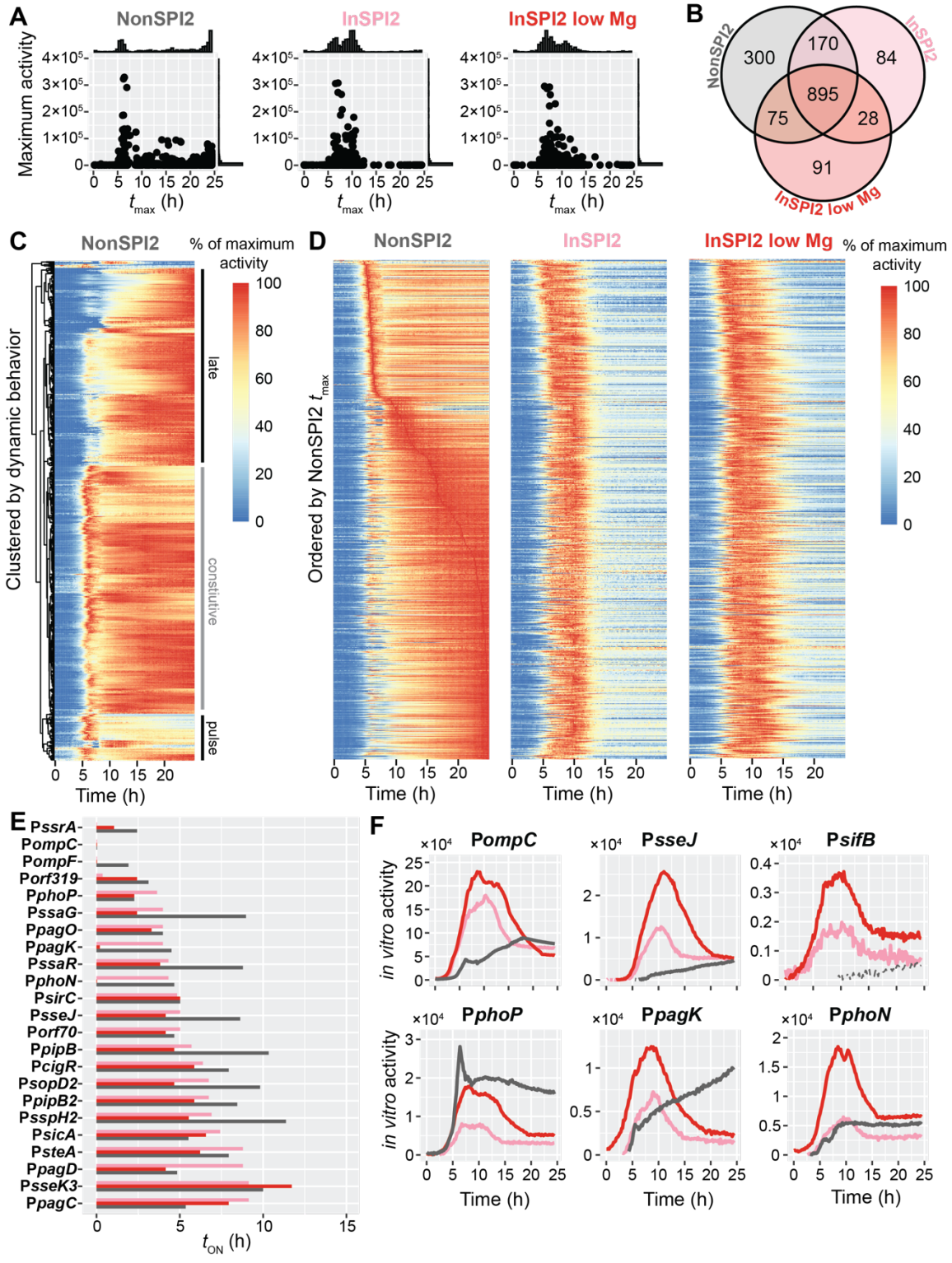

Figure 2: **Reporter library reveals system-level shifts in promoter activity dynamics in macrophage-mimicking media.**

A) Comparisons of time to maximum activity (t_{max}) and maximum promoter activity in NonSPI2 (left), InSPI2 (middle), and InSPI2 low Mg (right). Shown at the top and right are histograms of each quantity.

B) Venn diagram of all unique and shared ON promoters in NonSPI2 (grey, top left), InSPI2 (pink, top right), and InSPI2 low Mg (red, bottom).

C) Promoter dynamics in NonSPI2 for the 895 promoters that turned ON in all three media in (B). Each promoter profile (row) was normalized to its own maximum. Color represents the percentage of maximum activity. Profiles were clustered using a centroid-based method to highlight distinct qualitative behaviors (i.e., constitutive, late, pulse).

D) Promoter dynamics for the 895 promoters that turned ON in all three media in (B) in NonSPI2 (left), InSPI2 (middle), and InSPI2 low Mg (right). Each promoter profile (row) was normalized to its own maximum. Color represents the percentage of maximum activity. All heatmaps are ordered by ascending t_{max} in NonSPI2 to illustrate changes in promoter dynamics in SPI2-inducing media.

E) Time to initial activity (t_{ON}) for virulence-related genes (rows) in InSPI2 (pink), InSPI2 low Mg (red), and NonSPI2 (dark grey). Only promoters that showed activity in all three conditions were included. Reporters were ordered by ascending t_{ON} in InSPI2.

F) Promoter activity dynamics for six virulence reporters (*ompC*, *sseJ*, *sifB*, *phoP*, *pagK*, *phoN*) in NonSPI2 (grey), InSPI2 (pink), and InSPI2 low Mg (red). Activity is reported as GFP (parent-subtracted to account for autofluorescence) normalized to blanked OD_{600} (to account for changes in cell number). A promoter was defined as ON based on comparison to a dynamic estimate of background noise (**Methods**). ON activity is denoted by solid lines, whereas OFF activity is denoted by dashed lines.

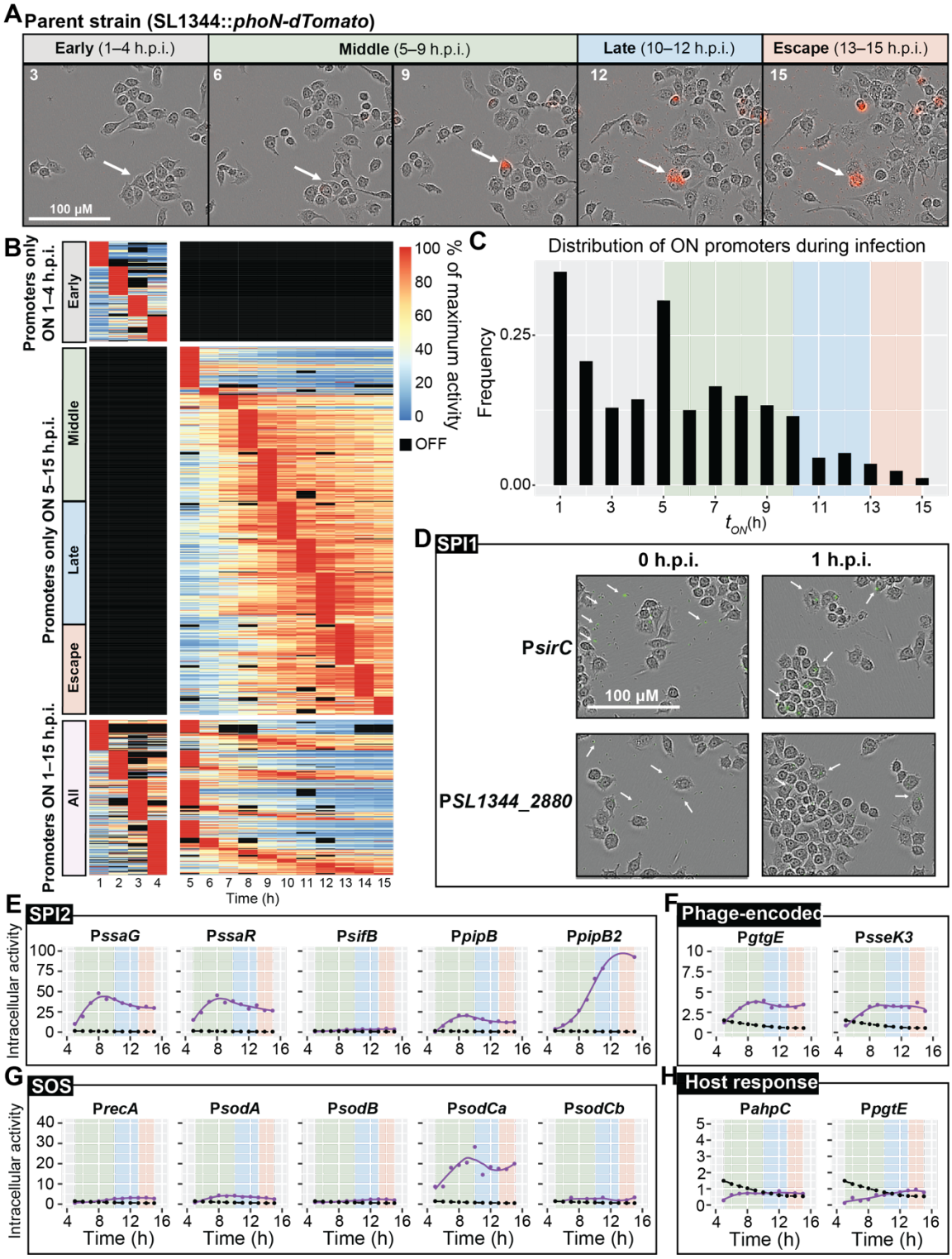

Figure 3: Intracellular *S.* Tm exhibits time-dependent regulation throughout macrophage infection.

A) Time-lapse images of the parent strain of the *S.* Tm reporter library, SL1344::*phoN-dTomato*. Shown are phase-contract images overlaid with the dTomato signal, which is produced once *phoN* is induced after responding to SCV maturation. Numbers in the upper left indicate the time in hours. The infection was binned into multiple stages of infection: early (0–4 h.p.i.), middle (5–9 h.p.i.), late (10–12 h.p.i.), and escape (13-–5 h.p.i.). White arrows indicate the same infected macrophage tracked over the 15 h interval.

B) Dynamics for 1,007 active promoters in macrophages ordered by ascending t_{max}. Each promoter profile (row) was normalized to its own maximum. Color represents percentage of maximum activity. Promoters are ordered by ascending t_{max} to show that maximum activity is collectively attained across all stages of infection.

C) The distribution of times at which activity was initially detected (t_{ON}) for the 1,007 ON promoters. The background colors for the plots represent the stage of macrophage infection as early (grey), middle (green), late (blue), and escape (orange).

D) Time-lapse images of reporters for two promoters in the SPI locus (P*sirC* and P*SL1344_2880*) that are ON during the early stage of macrophage infection. Shown are phase-contrast images overlaid with the GFP and dTomato channels (no dTomato signal was detectable at this early timepoint due to the dependence of *phoN* expression on SCV maturation). Several GFP-positive bacteria were present at the initial time points for pre- and post-invasion (0 and 1 h.p.i., respectively).

E) Promoter activity dynamics for several promoters regulating the expression of SPI2-relevant genes between 5–15 h.p.i. Intracellular macrophage activity (parent-subtracted GFP normalized by background-subtracted dTomato) is shown in purple and the dynamic background threshold is shown in black. Points are measurements, and lines are LOESS curve fits. The background colors for the plots represent the stage of macrophage infection as middle (green), late (blue), and escape (orange).

F) Activity dynamics for promoters regulating the expression of prophage-encoded genes between 5–15 h.p.i.

G) Activity dynamics for promoters that are known to regulate the SOS response between 5–15 h.p.i.

H) Activity dynamics for promoters that reach a maximum in the later stages of infection when *S*. Tm is preparing for escape during host lysis between 5–15 h.p.i.

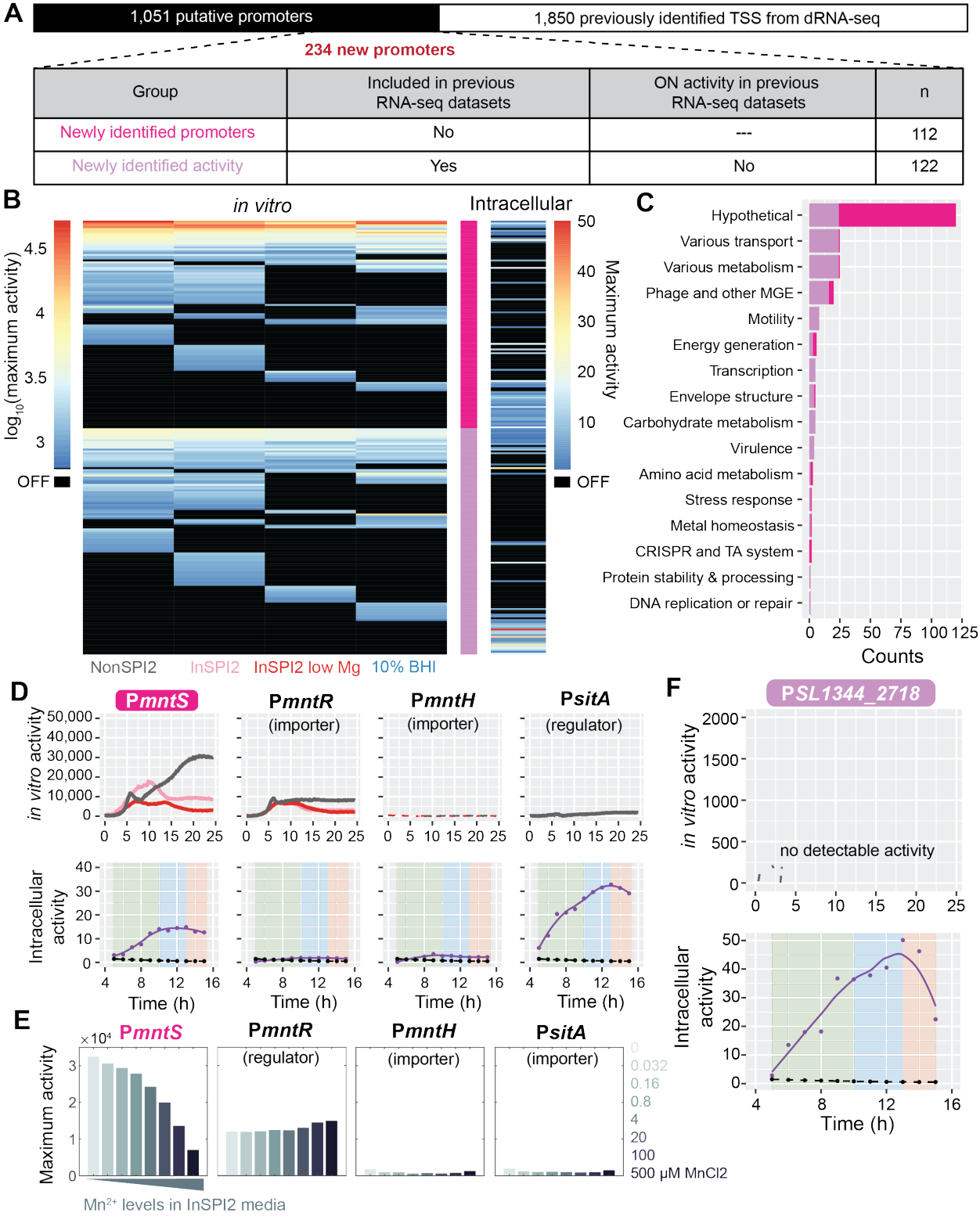

Figure 4: Comparison between *in vitro* growth and intracellular macrophage infection reveals promoters important for manganese regulation.

A) Division of the 234 novel promoters identified in our screens into two categories: “newly identified promoters” were not included in previous RNA-seq datasets, and thus do not have currently available expression data (pink); promoters with “newly identified activity” did not show activity in previous RNA-seq datasets across a compendium of *in vitro* and macrophage infection conditions (purple).

B) Normalized maximum activity for the 234 putative promoters that were computationally predicted but had not been previously experimentally validated. Maximum activity is shown for the *in vitro* conditions NonSPI2, InSPI2, InSPI2 low Mg, and 10% BHI (left) and intracellular macrophage infection (right). Black values denote OFF. Promoters are grouped by the categories in (A).

C) Functional categorization of the 234 novel promoters.

D) Promoter activity dynamics for P*mntS*, P*mntR*, P*mntH*, and P*sitA*. P*mntS* is in the “newly identified promoters” group. Top: *in vitro* activity (parent-subtracted GFP normalized by background-subtracted OD_{600}) for NonSPI2 (grey), InSPI2 (pink), and InSPI2 low Mg (red). Solid lines denote ON activity, and dotted lines denote OFF activity. Bottom: intracellular macrophage activity (parent-subtracted GFP normalized by background-subtracted dTomato) is shown in purple, and the dynamic background threshold is shown in black. Points are measurements, and lines are LOESS curve fits. The background colors for the plots represent the stage of macrophage infection as middle (green), late (blue), and escape (orange).

E) Maximum promoter activity for P*mntS*, P*mntR*, P*mntH*, and P*sitA* in InSPI2 medium supplemented with 0 to 500 μM $MnCl_2$.

F) Promoter activity dynamics for P*SL1344_2718*, which is in the group of promoters with “newly identified activity.” Top: *in vitro* activity (parent-subtracted GFP normalized by background-subtracted OD_{600}) for NonSPI2 (grey), InSPI2 (pink), and InSPI2 low Mg (red). No activity was detected in any *in vitro* conditions. Bottom: intracellular macrophage

activity (parent-subtracted GFP normalized by background-subtracted dTomato) is shown in purple, and the dynamic background threshold is shown in black. Points are measurements, and lines are LOESS curve fits. The background colors for the plots represent the stage of macrophage infection as middle (green), late (blue), and escape (orange).

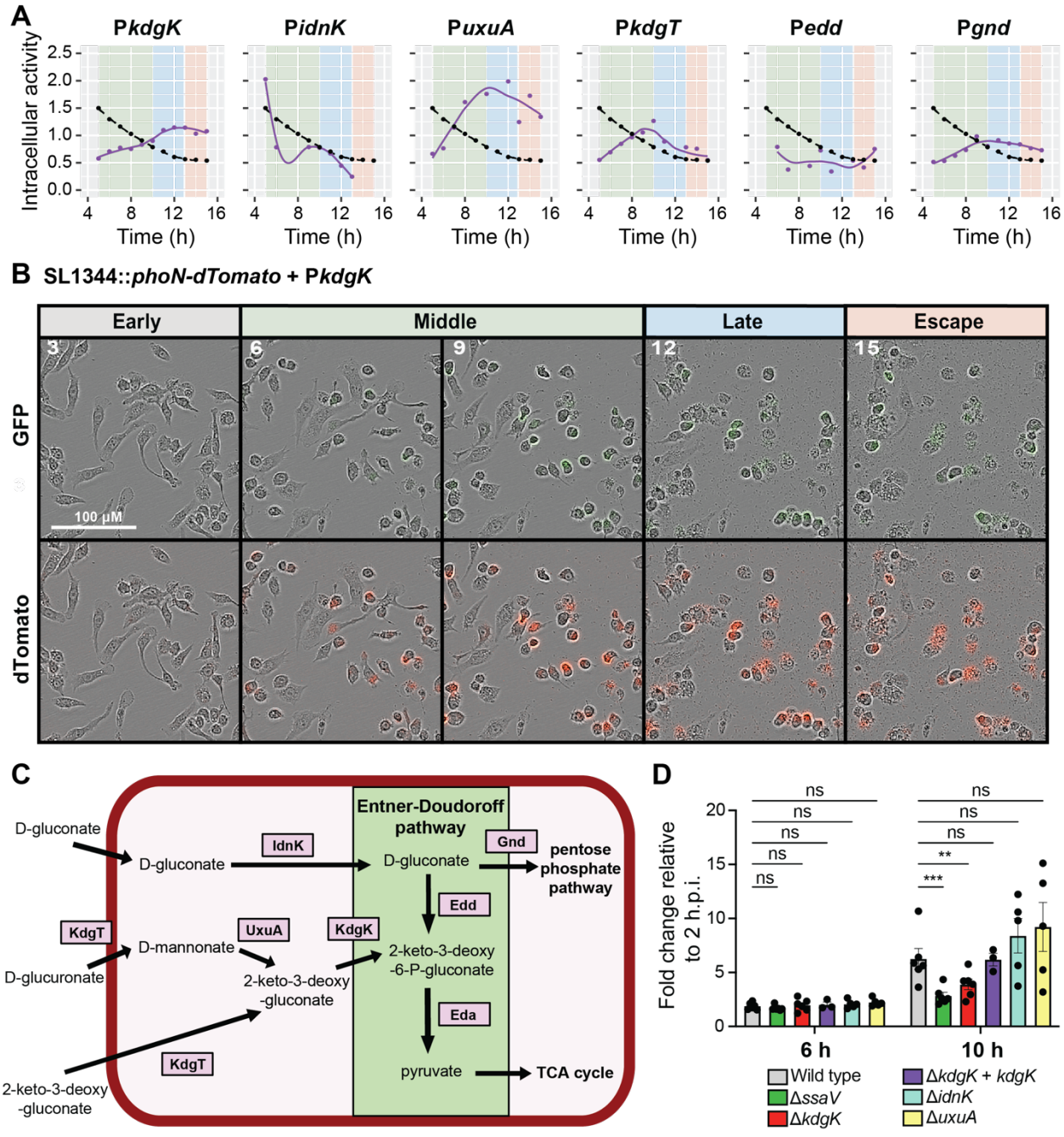

Figure 5: *S.* Tm depends on the Entner-Doudoroff (ED) pathway during later stages of macrophage infection.

A) Normalized GFP dynamics from *S.* Tm in infected macrophages for several promoters regulating the expression of genes related to the ED pathway (*kdgT*, *kdgK*, *edd*, *uxuA*,

idnK, *gnd*) between 5–15 h.p.i. Intracellular activity is parent-subtracted GFP normalized by background-subtracted dTomato. Points are measurements and lines are LOESS 5 ure curve fits. Each reporter was compared to the background threshold (black dotted line). The background colors for the plots represent the stage of macrophage infection: middle (green), late (blue), and escape (orange).

C) Time-lapse images of the activity of the P*kdgK* reporter strain during macrophage infection. Shown are phase-contrast images overlaid with the GFP (top) or dTomato (bottom) signal. Numbers in the upper left indicate the time in hours.

D) Catabolic pathways of several sugar acids including the ED pathway (highlighted in green).

E) Macrophages were infected with *S*. Tm mutant strains carrying the plasmid pFCcGi. Macrophages were harvested, fixed, and stained at 2, 6, and 10 h p.i. for analysis by flow cytometry. Fold replication was determined by comparing the ratio of mean GFP to mean mCherry signal at 6 and 10 h.p.i. to the ratio at 2 h.p.i. for each mutant. Error bars represent 1 standard error of the mean (SEM) for n=5 independent experiments for each mutant and n=3 independent experiments for the Δ*kdgK*+*kdgK* complementation strain. Multiple unpaired t-tests were conducted for each strain relative to wild type with a two-stage step-up method for multiple hypothesis correction. **: p<0.01; ***: p<0.001.